Superelasticity of Plasma- and Synthetic Membranes Resulting from Coupling of Membrane Asymmetry, Curvature, and Lipid Sorting

Jan Steinkühler,* Piermarco Fonda, Tripta Bhatia, Ziliang Zhao, Fernanda S. C. Leomil, Reinhard Lipowsky, and Rumiana Dimova*

Biological cells are contained by a fluid lipid bilayer (plasma membrane, PM) that allows for large deformations, often exceeding 50% of the apparent initial PM area. Isolated lipids self-organize into membranes, but are prone to rupture at small (<2–4%) area strains, which limits progress for synthetic reconstitution of cellular features. Here, it is shown that by preserving PM structure and composition during isolation from cells, vesicles with cell-like elasticity can be obtained. It is found that these plasma membrane vesicles store significant area in the form of nanotubes in their lumen. These act as lipid reservoirs and are recruited by mechanical tension applied to the outer vesicle membrane. Both in experiment and theory, it is shown that a "superelastic" response emerges from the interplay of lipid domains and membrane curvature. This finding allows for bottom-up engineering of synthetic biomaterials that appear one magnitude softer and with threefold larger deformability than conventional lipid vesicles. These results open a path toward designing superelastic synthetic cells possessing the inherent mechanics of biological cells.

J. Steinkühler[+], P. Fonda, T. Bhatia, Z. Zhao[++], F. S. C. Leomil,
R. Lipowsky, R. Dimova
Theory and Bio-Systems
Max Planck Institute of Colloids and Interfaces
Science Park Golm, Potsdam 14424, Germany
E-mail: jan.steinkuehler@northwestern.edu; dimova@mpikg.mpg.de
T. Bhatia
Department of Physical Sciences
Indian Institute of Science Education and Research Mohali
Sector 81, Knowledge City, Manauli, SAS Nagar, Punjab 140306, India
F. S. C. Leomil
Departamento de Biofísica
Universidade Federal de São Paulo
São Paulo 043039-032, Brazil

The ORCID identification number(s) for the author(s) of this article can be found under https://doi.org/10.1002/advs.202102109

[+]Present address: Department of Biomedical Engineering, Northwestern University, Evanston, IL 60657, USA

[++]Present address: Leibniz Institute of Photonic Technology, Jena 07745, Germany

1. Introduction

The concept of compartmentalization is central to living systems. A ubiquitous compartment-forming element in cells are lipid bilayers, with the most prominent example of the outer cell membrane or plasma membrane (PM). The PM is a complex biomaterial that has to support dynamic shape changes of the cell and its mechanical failure would result in cell death, highlighting the importance of PM mechanical properties. PM elasticity has been probed using micropipettes,[1] tube-pulling, and atomic force microscopy indentation experiments.[2,3] These methods probe the in situ response of the PM to mechanical challenges and are thus informative of the physiologically relevant response in the context of the living cell. For example, in situ experiments probe the PM adhesion to the cell cortex and recruitment of membrane material via exocytosis.[4]

This interwinding represents a challenge for reductionist approaches that try to rebuild some of the cellular functionality for "synthetic cells," because engineering approaches rely on the definition of well-characterized parts. Here, we address these challenges by isolation of plasma membrane sheets by chemical induction, a method that has been used before to study phase behavior[5] and bending rigidity of plasma membranes.[6] In contrast to previous studies, we describe conditions that lead to the reconstitution of large-scale area reservoirs. Tension-induced recruitment of these area reservoirs proceeds by an apparent, or superelastic, response far exceeding the deformability of usual lipid bilayers but representing a characteristic feature of living cell plasma membranes. By detailed comparison of experiment and theory, we isolate the curvature-elastic parameters that allow for the observed superelastic behavior. Informed by these results we engineered a lipid-only vesicle analogue that appears one magnitude softer and with threefold larger deformability than conventional lipid vesicles, thus bringing synthetic biology approaches one step forward toward building synthetic cells.
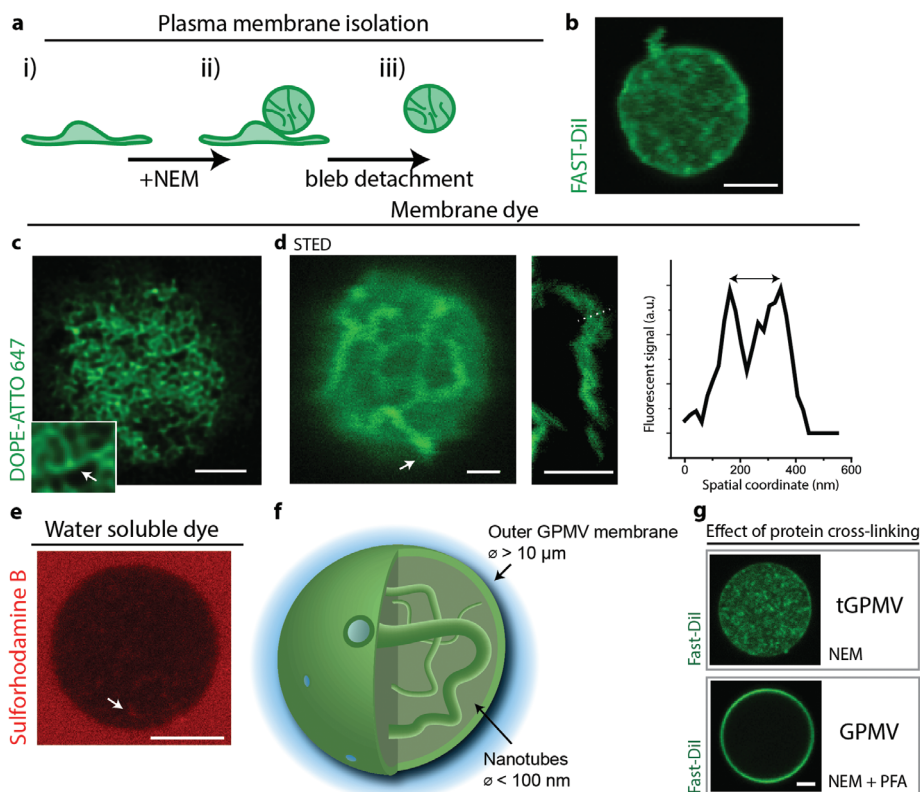
Figure 1. a) Extraction and isolation of plasma membrane by incubation of U2OS cells with *N*-ethylmaleimide (NEM). Scale bar: 5 μm. b) Membrane extracts were isolated and labeled with fluorescent membrane dye (FAST-DiI) (shown in green). c) High-resolution imaging of the internal structures by deconvolution of confocal images reveals a dense lipid network. Possible three-way branches are shown in the inset. d) STED microscopy of internal structures found in the lumen of the vesicles. Left: Nanotubes appear to be connected to the outer membrane. Middle: Image of one tube. Right: Fluorescence intensity plot along the dotted line indicated on the middle image. The two peaks correspond to the nanotube walls and exemplify a nanotube radius of about 100 nm. Scale bars: 1 μm. e) Diffusion of water-soluble dye added to the outer solution into the nanotubes. The arrow shows signal detected in the water-filled nanotube interior. Scale bar: 5 μm. f) Sketch of the overall GPMV structure (vesicle and nanotube diameter not to scale). g) Effect of crosslinking chemical PFA on plasma membrane vesicles. We term tGPMV extracts to those that reconstitute a tubular lipid network. Scale bar: 5 μm.

2. Results

2.1. Isolation of Structurally Conserved Plasma Membrane Leads to Formation of Vesicles with Cell-Like Elastic Response

After chemical cleavage of the cytoskeleton-PM anchors induced by incubation with *N*-ethylmaleimide (NEM), turgor pressure leads to the formation of spherical blebs called giant plasma membrane vesicles (GPMVs). These vesicles reconstitute PM lipids and membrane proteins,[7] and encapsulate soluble cytosolic components (**Figure 1**a and the Experimental Section).[8,9] GP-MVs were isolated from the cells and stained with the membrane dye FAST-DiI (see the Experimental Section for details). Unexpectedly, fluorescence intensity not only was observed on the outer (spherical) GPMV membrane segment, but also appeared in the vesicle lumen (Figure 1b). We observed this effect both when fluorescent dye was introduced to the cells before GPMV extraction or to unlabeled GPMVs after extraction. Deconvolution and super-resolution imaging (stimulated emission depletion, STED) revealed the presence of a tubular lipid network which is contained within the isolated GPMVs and connected to the outer membrane (Figure 1c). In some vesicles, the tubular network was

found to be very dense and possibly branched (Figure 1c inset). The diameter of the lipid nanotubes appeared to be mostly below the resolution limit of our STED setup (about 50 nm), but some tubes were wide enough to be directly resolved by STED measurements (Figure 1d). To aid interpretation of the imaging results, a water-soluble dye was added to the outer aqueous solution. Fluorescence signal from the water channels formed by the nanotubes provided direct evidence for the tubular structure and connection to the outer membrane (sulforhodamine B dye in Figure 1e). Together, this confirms that GPMVs isolated in the conditions employed here, reconstitute a nanotubular lipid network (Figure 1f), which is similar to tubular structures found in cells.[10,11] Curvature elasticity arguments suggest that coexistence of the outer, weakly curved membrane segment, and the highly curved nanotubes requires that the membrane exhibits preferred, or spontaneous curvature, in the order of $m_{tubes} > 1/200$ nm$^{-1} = 5$ μm^{-1}, stabilizing the highly bent lipid bilayer.[12] Similar spontaneous curvature values were shown to be generated by adsorption of curvature-inducing BAR domain proteins to the bilayer.[13] Indeed proteomics indicates that BAR-domain proteins are present in GPMVs[9] and are known drivers of membrane tubulation in vitro and in vivo.[14]

Consistent with protein coverage on the cytosolic leaflet of the nanotubes, addition of the protein crosslinker paraformaldehyde (PFA) led to crosslinking of the nanotubes. This effect was exploited to immobilize and thus obtain the high-resolution images of the otherwise dynamically fluctuating nanotube network shown in Figure 1c,d (also see the Experimental Section).

However, if the crosslinking chemicals were present during plasma membrane extraction, the GPMVs interior appeared free from any fluorescence signal of membrane dye (Figure 1g and the Experimental Section), suggesting that the excess lipid material was retained inside the cells by the crosslinking agent. Consistent with previous reports,[15] the vesicles isolated in crosslinking conditions sometimes appear to be permeable to the water-soluble dye. However, this effect leads to homogenous dye distribution in the vesicle lumen and can be clearly distinguished from the structured signal from internal nanotubes shown in Figure 1e. Previous experiments using GPMVs were often conducted in the presence of crosslinkers,[16] and to distinguish the protocol used here, we term vesicles reconstituting a tubular lipid network tGPMVs.

2.2. Tension Retracts Nanotube Network to Outer Membrane

As long as all membranes remain fluid and the nanotubes in the vesicle lumen are connected to the outer membrane, it should be possible to retract them to the outer vesicle membrane by exposing them to mechanical tension as previously shown.[17] Indeed, when tGPMVs were aspirated into glass capillaries, similar to those used for elastic probing of cells[18] and lipid vesicles,[19] we were able to induce large-scale elastic deformations corresponding to about 20–25% increase of the initial apparent outer membrane area (**Figure 2**a). At a fixed tension tGPMVs remained stable with a constant membrane area of the outer segment and without indication of hysteresis along the trajectory (Figure 2a). For comparison, GPMVs that were isolated in conditions that do not reconstitute a nanotube network, appeared three orders of magnitude stiffer and did rupture at small area strains of about 3%, in a manner reminiscent of pure lipid bilayers[19] (Figure 2b). When compared to literature data of micropipette aspiration of neutrophil cells,[18] it becomes clear that tGPMV elasticity appears to be much more similar to that of intact cells rather than other biomimetic systems. While elasticity and area regulation in cells is certainly orchestrated by a range of (active) processes, including the actomyosin cortex and exocytosis of small vesicles, our results suggest that the plasma membrane composition and morphology itself is poised to exhibit an elastic response matching the cortical tension. While this behavior has interesting implications for cell biology, we aimed to understand the physical mechanism that enable PM superelasticity.

2.3. Nanotube Retraction Leads to Compositional Change of the Outer Membrane Segment

It seems likely that the extraordinary tGPMV deformability proceeds by the recruitment of the nanotubes into the outer membrane. Indeed, recruitment of membrane material from the nanotube could be directly visualized by fluorescence lifetime measurements (FLIM): FAST-DiI lifetime is a measure of membrane composition and is related to the order parameters of the acyl chain over a wide range of membrane composition, but not to membrane curvature alone (Figure S1, Supporting Information; ref. [21]). Color coding for FAST-DiI fluorescence lifetime immediately reveals two distinct populations of fluorescence lifetimes between the outer membrane segments and nanotubes (Figure 2c), indicating a stark contrast in composition and lipid order.

Next, we observed the fluorescence lifetime of the outer membrane segment upon aspiration of a tGPMV. We found that the fluorescence lifetime of the dye in the outer membrane segment shifts by a value of Δ toward the lifetime found in the nanotubes (Figure 2c). Control aspiration experiments on GPMV (Figure 2c) exhibit no such shift in lifetime ($\Delta \approx 0$). We also attempted to measure the corresponding shift in fluorescence lifetime in the nanotube network. Compared to the outer membrane segment, the resolution is limited by the lower and more heterogenous signal. On average, a small shift toward the outer membrane lifetime was obtained, which was not found to be significantly different from zero (Figure S2, Supporting Information). Thus, we speculate that the nanotube network acts as a large reservoir of constant membrane composition. Similar to constructing a tie line in a phase diagram using the lever-rule, the exact partitioning behavior will depend on the relative area fractions of outer membrane segment and nanotubes.

In summary, these measurements represent direct evidence of mixing of the two membrane segments with tension. Essentially, we witness a continuous phase change of the outer membrane as a response to an increase in aspiration pressure and membrane tension.

2.4. Outer Membrane Segment and Nanotubes Have Distinct Membrane Compositions

The difference in composition between nanotubes and the outer membrane segment will be crucial for the interpretation of the tGPMV "superelastic" response and was corroborated by further experiments. Co-staining with the dyes FAST-DiI and DiD reveals segregation of the two lipid-like molecules between the outer membrane segment and the highly curved nanotubes (Figure 2d). FAST-DiI and DiD have similar molecular structure, except that FAST-DiI exhibits a double bond in the acyl chain. Compared to this small chemical difference, a strikingly different partitioning of the two dyes is obtained. In fact, within the detection limit of our experimental setup, which approaches single-molecule sensitivity, no fluorescence signal from DiD in the nanotube membrane segment is detected. Interestingly, the two dyes were shown to segregate during endocytosis in cell experiments,[22] but dyes of similar acyl chain chemistry have shown neglectable sorting in synthetic vesicles before.[23] Prompted by this finding, we investigated the nanotube composition using a series of typical PM fluorescent stains. The nanotube segment is rich in membrane protein as seen by NHS-Alexa 647, which forms complexes with protein primary amines. Nanotubes were found negative for Transferrin marker, indicating absence of clathrin coats, and were also found negative for Annexin A5 binding. Nanotubes were positive for staining with Cholera toxin subunit B (CT-B) (Figure 2e). These results are
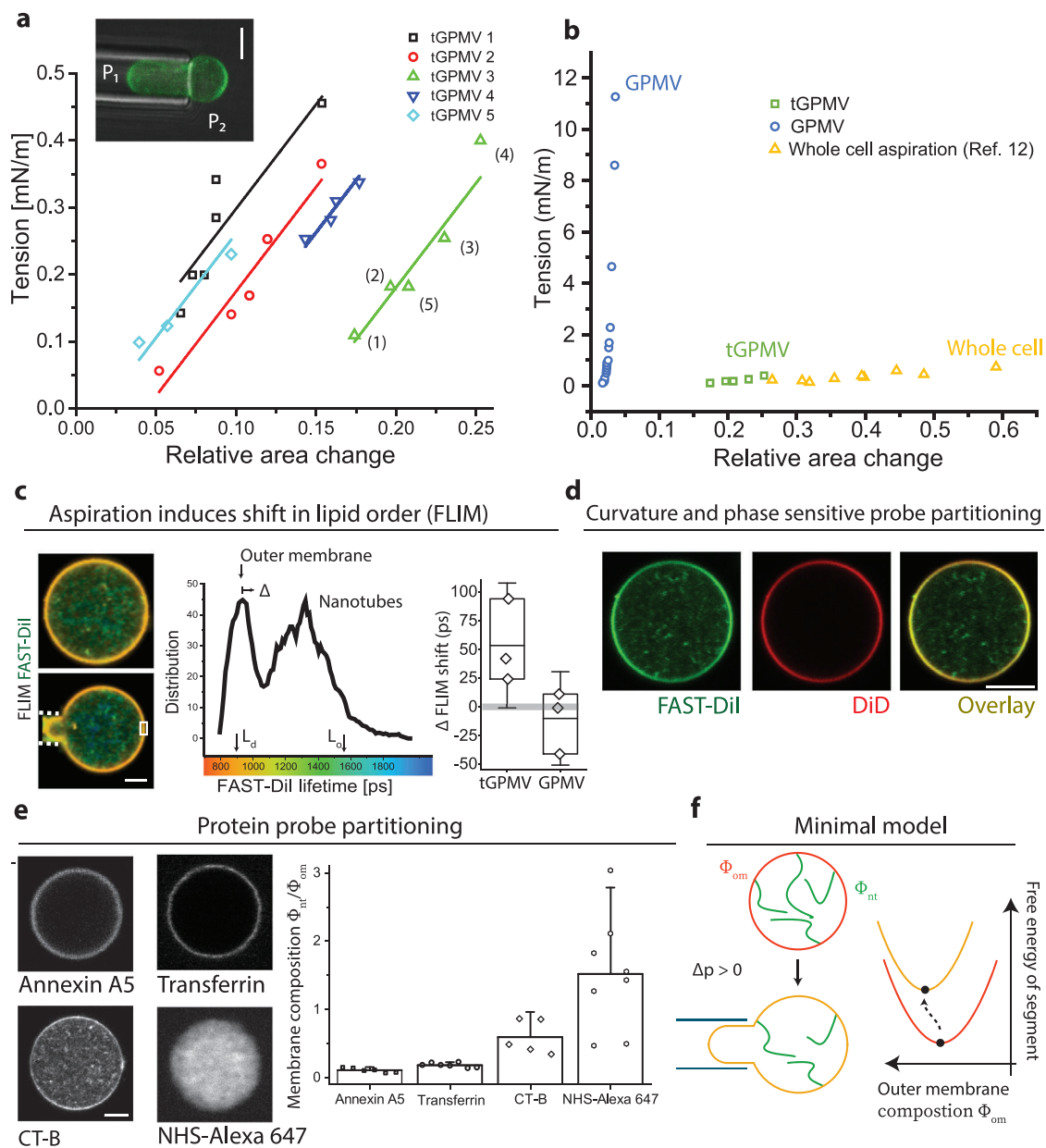
Figure 2. a) Vesicle projected (outer) area from micropipette aspiration of individual tGPMVs (color-coded) at varying pressure differences $\Delta P = P_2 - P_1$, the tension is calculated from the Laplace pressure as $\frac{R_p \Delta P}{2(1 - R_p/R_v)}$, where R_p and R_v are the corresponding pipette and spherical membrane segment radii. The numbers in brackets indicate the experimental sequence of applied pressures. b) Comparison between apparent elastic moduli obtained for GPMVs and tGPMVs (measured here), and neutrophils (data from ref. [20]). c) FLIM data: color code indicates FAST-DiI fluorescence lifetime in a free tGPMV (top image) and when aspirated (bottom image), white dashed lines indicate micropipette. The histogram shows lifetime distribution. Upon application of a low membrane tension (0.7 ± 0.3 mN m^{-1}), the lifetime of the outer membrane segment (data collected in the region of interest marked by the white rectangle) is shifted to higher values by Δ. In the right panel, we compare this tension-induced change (Δ) in tGPMVs and GPMVs. Each data point represents an independent experiment. Note that the fluorescence lifetime in the nanotube network (as evaluated from measurements in the central vesicle part) is not changing substantially (see Figure S2 in the Supporting Information). d) Co-staining of the same tGPMV with membrane dyes FAST-DiI and DiD (green and red channel) and overlay: DiD is expelled and sorted out from the nanotubes. e) Staining of the external leaflet of tGPMV with protein (primary amines) binding NHS-Alexa 647 and fluorescently conjugated annexin A5, transferrin, and cholera toxin subunit B (CT-B) (see the Experimental Section for details). Bar plot shows fluorescent signal ratio between outer membrane and the tubular network of tGPMVs. All vesicle diameters were between 10 and 30 µm. f) Sketch of the model of outer membrane segment with composition Φ_{om} and lipid nanotube reservoir of composition Φ_{nt}. Aspiration leads to unfavorable lipid–lipid interaction in the outer membrane segment that contribute to the apparent elastic response.

ADVANCED
SCIENCE NEWS

www.advancedsciencenews.com

ADVANCED
SCIENCE
Open Access

www.advancedscience.com

consistent with cylindrical morphology of the nanotubes (shown to reduce Annexin A5 binding affinity[24]), which, as shown in cells, are stained by nonclathrin mediated endocytosis marker CT-B.[10,25] Taken together these results indicate strong partitioning of lipids and protein in the curvature field of the two membrane segments, effectively coupling membrane composition, phase state, and curvature.[26–28] The partitioning of PM lipids between highly curved nanotubes and outer membrane segments is in agreement with predictions from molecular dynamics simulations informed by plasma membrane lipidomics,[29] further corroborating our observations. In fact, we could have arrived at a similar conclusion without the need for aspiration experiments: upon osmotic deflation, the outer membrane segment starts to fluctuate with optically resolvable amplitudes, indicating a membrane tension in the entropic regime.[6] This implies that the outer membrane is close to its preferred membrane curvature.[30] Taking tGPMV diameter of about 5 μm yields $m_{outer} < 1/5\ \mu m^{-1}$ for the spontaneous curvature of the outer membrane, while the nanotubes have a spontaneous curvature of $m_{tubes} > 5\ \mu m^{-1}$ as implied by tube diameter below the optical resolution. Thus, tGPMVs must exhibit two membrane domains of distinct curvature and composition.

Combining all results, we see that when the plasma membrane is left to relax and equilibrate from cytoskeletal pining, it generates vesicles that consist of two membrane domains with remarkably different composition and curvature. Together with previous studies on the miscibility temperature of GPMVs[5] and critical fluctuations,[31] our studies complement the thermodynamic characterization of plasma membrane extracts.

2.5. Membrane Curvature and Domains Separation Act to Stabilize Area Reservoirs and Lead to Superelastic Response

To explain how the multicomponent nature of tGPMVs is responsible for their cell-like elasticity, we have adopted a minimal working model based on the observation that nanotubes have considerably different composition with respect to the outer membrane (Figure 2d,e) and that the composition of the outer membrane changes upon pipette aspiration (Figure 2c). The high curvature prevents a fraction of the PM molecules to enter the nanotubes, so that they can provide a reservoir for only a subset of the species present in the whole membrane. In the Supporting Information, we show how, in general, the compositional shift of the outer membrane induced by aspiration generates restoring forces due to curvature–composition interactions. These forces emerging from unfavorable lipid–lipid interactions can easily oppose any suction pressure, and prevent the development of droplet-like instabilities as observed in homogeneous tubulated GUVs.[17] For the range of relative area changes studied here, the measured aspiration tension has a general structure

$$\frac{\Delta P R_p}{2\left(1 - R_p/R_v\right)} \simeq \Sigma_{app} + K_{app}\frac{\Delta A}{A_0} \tag{1}$$

where A_0 is the outer membrane area before aspiration, ΔA is the area increase due to suction, Σ_{app} is a tension term, which depends on the composition of both domains, and K_{app} is the "apparent" elastic modulus (see Equation (S27) in the Supporting In-

formation). While in general K_{app} contains several contributions due to the different ways in which membrane composition can couple to curvature, we can show that, to explain the measured value of 3.1 ± 0.2 mN m⁻¹ (see Figure 2a), the leading term in the modulus has the simple form

$$K_{app} \simeq \left(\Phi_{om} - \Phi_{nt}\right)^2 \frac{\partial^2 e\left(\Phi_{om}\right)}{\partial \Phi^2} \tag{2}$$

where Φ_{om} and Φ_{nt} are two order parameters characterizing the composition of the outer membrane and nanotubes, while $e(\Phi_{om})$ is the free energy density per unit area of a membrane with composition Φ_{om}. Using mean-field theory estimate for the energy, we calculate that a lipid–lipid interaction strength of the order of the thermal energy (see Equation (S41) in the Supporting Information) can reproduce the measured value of Σ_{app}, consistently with previous experimental values.[32] The simple structure of Equation (2) when compared with the dependency of Σ_{app} on the nanotube composition can explain why the observed trajectories in Figure 2a have the same slope but different intercept (see Equation (S25) in the Supporting Information).

In principle, there might be additional energetic contributions arising during aspiration, due to, e.g., scaffolding of proteins,[33] line tension, the finite size of the nanotube network, crosslinking between the nanotubes, or changes in the elastic parameters of the membrane itself.[34] All these effects would likely act to increase K_{app} further. Here, we have shown that the observed remixing of lipids between nanotube reservoir and the outer vesicle is sufficient to explain the magnitude of the measured apparent elastic response. Compared to vesicles without area-reservoirs, the described effect has much lower energetic cost than tension-induced changes to the preferred area per lipid. This distinguishes our finding from the conventional elasticity of simple lipid membranes, which has a mechanical, rather than chemical, origin and is similar to the stiff stretching response of GPMVs without nanotube network (Figure 2b). Another limit case of our model case are vesicles with nanotubes of the same composition as the outer segment ($\Delta\Phi = 0$), in this case, K_{app} vanishes, consistently with previous experiments.[17] We conclude that tGPMVs are able to withstand much larger deformations as their elastic response is not limited by the increase in mechanical membrane tension, but by the available lipid material in the nanotubes.

2.6. Bottom-Up Construction of Superelastic Vesicles

After we have identified the physics behind superelasticity in tGPMVs, we demonstrate that vesicles with similar size and elastic properties can be created in the lab de novo from synthetic lipids. In synthetic giant unilamellar vesicles (GUVs) nanotubes are generated by membrane spontaneous curvature, which is induced by membrane asymmetry.[12,35,36] Following a method reported previously by us, membrane asymmetry is generated by sorting of the charged lipid DOPG (1,2-Dioleoylphosphatidylglycerol) between membrane leaflets[37] (Figure S3, Supporting Information). Upon osmotic deflation, DOPG:cholesterol GUVs form inward-pointing nanotubes, adopting a similar vesicle morphology to tGPMVs. However, in
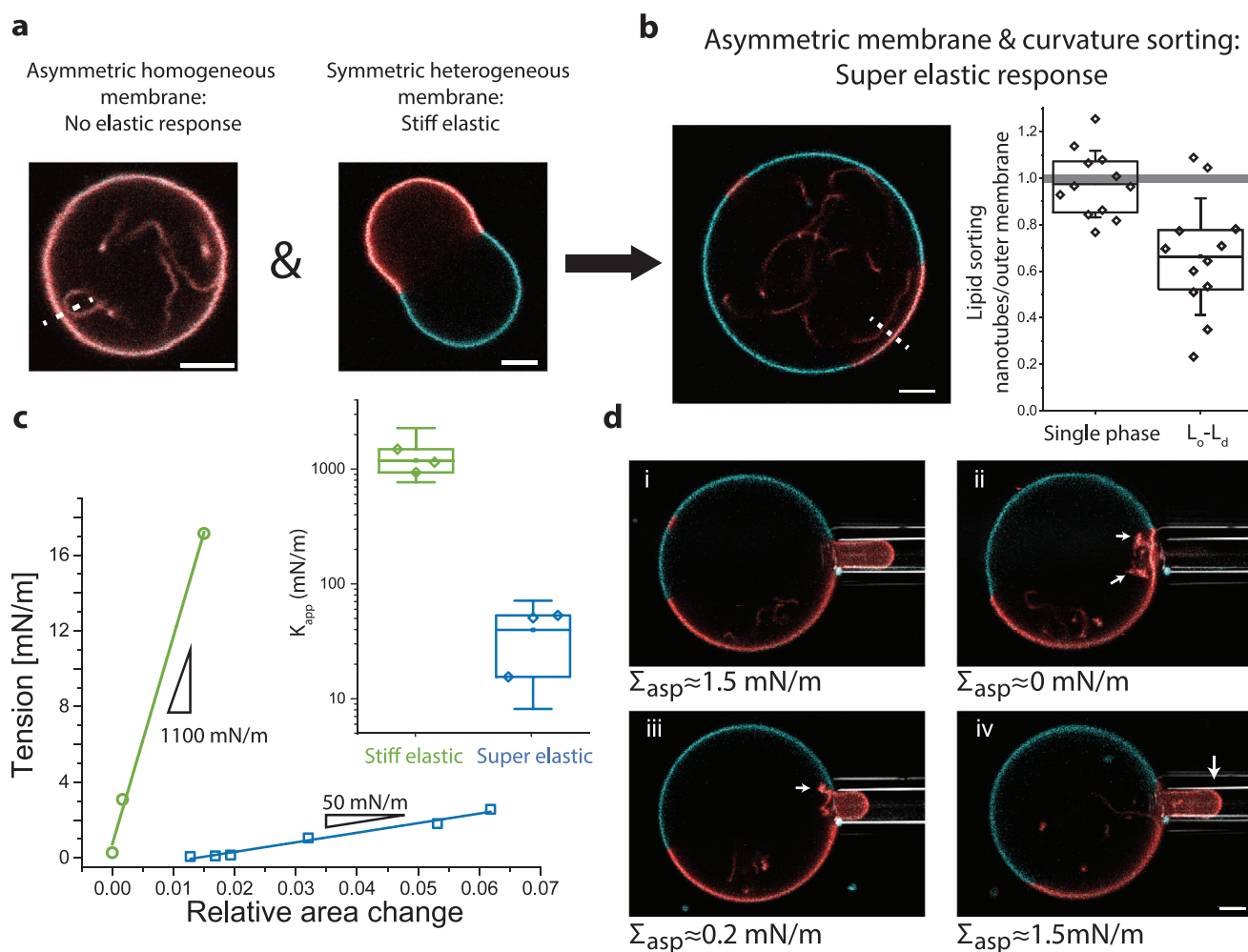
Synthetic reconstitution

Figure 3. a) Tubulated homogenous DOPG:cholesterol GUV with asymmetric membrane and heterogenous symmetric DOPG:SM:cholesterol GUV. In the second image, cyan color shows TopFluor-cholesterol (liquid ordered) and red DiIC:18 (liquid disordered). b) Asymmetric and heterogenous 3:5:2 DOPG:SM:cholesterol tGUV. The plot shows normalized membrane composition between outer liquid disordered membrane segment and nanotube (measured along the white dashed line) for single phase and L_o–L_d phase separated GUVs. c) Micropipette aspiration data of nontubulated symmetric (green) and tubulated asymmetric (blue) DOPG:SM:cholesterol GUVs of the same overall composition. Inset: Apparent elastic constant K_{app} deduced from the area change with applied tension. Note the logarithmic scale. Each data point indicates an independent experiment. d) Reversibility of recruitment of nanotubes from phase separated GUV. Time series from (i)–(iv) where the intermediate aspiration at tension (iii) was equilibrated before suction pressure increases. All scale bars are 5 µm.

contrast to tGPMVs, DOPG:cholesterol GUVs exhibit nanotubes of the same composition as that of the outer membrane segment (**Figure 3**a,b—red data). Upon application of a small negative pressure difference, nanotubes in DOPG:cholesterol GUVs flow into the outer membrane at constant tension. As studied previously, constant membrane tension upon aspiration leads to a droplet-like instability of the GUV in the glass-capillary and no elastic response.[17] This behavior is indeed the limit case of $K_{app} \rightarrow 0$ studied here (see discussion of Equation (2)). To create an energetic cost for the mixing of nanotubes and outer membrane lipids, we introduce sphingomyelin (SM) as a third membrane lipid. Sphingomyelin tends to form a liquid ordered phase with cholesterol and segregates away from the liquid disordered DOPG-rich phase, leading to lipid liquid–

liquid phase separation.[38] Proximity to the liquid–liquid miscibility gap was previously shown to enhance lipid sorting in pulling experiments of force induced nanotubes.[34,39] Indeed, spontaneous lipid curvature sorting could be visualized by dye-labeled cholesterol and phospholipid analogues: in phase separated tGUVs, the dye intensity ratio between L_d segment of the outer membrane and L_d nanotube segment shows a compositional difference between the two membrane segments (Figure 3b). As expected, in control experiments on single-phase GUVs lipid sorting is weak and the nanotubes appear to have the same membrane composition as the outer membrane segment (Figure 3b).

Consistent with our hypothesis, only in asymmetric phase-separated tGUVs tension-induced nanotube retraction ascribes

a superelastic response: Aspirated DOPG:SM:cholesterol tGUVs appear over an order of magnitude softer and about three times more deformable compared to the bare symmetric DOPG:SM:chol GUVs without any area reservoirs (Figure 3c). Both types of GUVs have the same overall membrane composition, but exhibit a subtle nanoscopic structural difference, namely, in their membrane asymmetry. The deformations in tubulated GUVs were reversible, allowing for recruitment and re-forming of nanotubes (Figure 3d).

3. Discussion

We found that structurally intact PM isolated from cells shows similar elastic properties to cells when probed by micropipette aspiration. We demonstrate that this is due to the presence of a network of lipid nanotubes with different composition, and compositional heterogeneity reminiscent of liquid–liquid coexisting phases. Plasma membrane extracts not only exhibit planar phase separated domains[5] but are positioned to couple phase state and membrane curvature. While we believe that the high density of the tGPMV nanotube network is formed due to the unphysiological isolation procedure and loss of cytoskeletal pinning and tension, these nanotubes nonetheless bear similarities to the CLIC/GEEC nanotubes found in vivo. Similar to tGPMV nanotubes, cellular nanotubes were found positive for the membrane dye FAST-DiI, negative for Transferrin marker and with a diameter of about 40 nm.[10] CLIC/GEEC nanotubes were implicated previously in PM tension regulation,[40] which is consistent with the tension magnitude leading to tGPMV nanotube retraction. We have shown that rebuilding tGPMV main features of nanotube formation, stabilized by membrane spontaneous curvature and lipid–lipid interactions, enables a bottom-up synthetic reconstitution of superelastic tGUVs. Liquid–liquid phase separated membranes were widely studied in their phase behavior at various temperatures, showing only weak influence of mechanical tension.[41] By introducing the coexistence of not only lipid domains, but also large differences in membrane domain curvature, we have obtained a novel synthetic membrane system, which, we anticipate, will exhibit rich isothermal phase behavior by tension changes. Typically lipid bilayer elastic response is linked to expansion of the bilayer/water interface from its preferred area, where the interfacial tension stems from the hydrophobicity of the lipid tails.[42] Here, we show that a different type of elastic response can be engineered using nanotubular lipid domains that act as area reservoirs. The elastic response is now determined by two control parameters of domain composition and lipid–lipid interactions. Compared to the relatively constant lipid tail to water hydrophobicity, our mechanism allows for large deformations and precise control over the elastic response. In addition, the studied mechanism provides us with the ability to sort and reorganize lipids and proteins on plasma membrane mimetics by application of minute mechanical cues. In this way, superelastic membranes are bound to have a wide applicability in engineering of synthetic cells.

Compared to established superelasticity of phase-changing metal alloys,[43] tGPMV and their synthetic reconstitution allow for extensive 3D remodeling, demonstrating the remarkable features of membrane fluidity.

4. Experimental Section

GPMV and tGPMV Generation and Isolation: PM blebbing was induced according to previously published protocols[16] with modifications: U2OS cells were cultured in DMEM medium (10% FBS, 1% Penn-Strep) to 70% confluency, washed three times with 5 mL phosphate buffered saline (PBS), incubated at 4 °C for 10 min in PBS (1 mL suspension was supplemented with 1 µL 10 mg mg^{-1} FAST-DiI or DID (Thermofisher) in ethanol for experiments shown in Figures 1b and 2a–d), washed three times in buffer (10 × 10^{-3} M HEPES, 150 × 10^{-3} M NaCl, 2 × 10^{-3} M CaCl$_2$, pH 7.4), and incubated for 1 h with 2 × 10^{-3} M NEM in buffer (1 mL). As indicated in the main text, in some experiments, tGPMV induction was suppressed by addition of 25 × 10^{-3} M PFA to the chemical NEM resulting in the formation of nontubulated GPMVs. PM blebbing induction with 2 × 10^{-3} M DTT and 25 × 10^{-3} M PFA in buffer yielded similar results, namely, GPMVs lacking a tubular network. Cells were incubated for an hour at 37 °C and GPMV/tGPMV were harvested. Here, special precaution was taken to minimize agitation of the flasks. Vesicles were isolated by single pipetting from slightly tilted T-75 flasks yielding 1 mL supernatant. This procedure minimized contaminations from dead cells and other debris. After additional staining steps (see below), the harvested GPMVs were left to stand upright in an Eppendorf tube (1.5 mL volume) to let vesicles sediment by gravity for at least 30 min. A 100 µL sample collected from the bottom of the tube was then further analyzed within 12 h of sample isolation.

General Sample Preparation: Coverslips were cleaned (rinsed with ethanol and Millipore water) and coated with bovine serum albumin (BSA) (incubated with 100 µL 1 mg mL^{-1} BSA for at least 30 min and washed with Millipore water). Between 30 and 50 µL of the tGPMV/GPMV solution was pipetted on the coverslip and sealed with a top cover glass separated by a spacer.

Staining with Water Soluble Dyes: Water soluble dye and conjugated proteins were prepared according to the manufactures instructions and incubated for 20 min with tGPMV and GPMV solutions after isolation from the cell culture to the following final concentrations: 400 × 10^{-6} M Alexa Fluor 647 NHS-Ester (Thermo Fisher), 2.5 × 10^{-6} M sulforhodamine B (Sigma), 16.7 × 10^{-9} M cholera toxin subunit B—Alexa Fluor 488 (Invitrogen), 130 × 10^{-9} M Human Transferrin—CF488A (Biotium), and 65 × 10^{-9} M annexin V—CF594 (Biotium).

High-Resolution Imaging: To obtain high-resolution images of the tubular network, the diffusive nanotube motion was suppressed by protein crosslinking. The crosslinker PFA was added to tGPMVs after isolation (with NEM) from the cell culture. Importantly, crosslinking was only effective if PFA was supplemented with 0.17 × 10^{-3} M Triton X 100 (Sigma-Aldrich) to increase membrane permeability. If the membrane was not labeled during plasma membrane isolation, 1 µL of 1 mg mL^{-1} solution in ethanol STED dye (ATTO 647N DOPE, Sigma-Aldrich) or FAST-DiI was added to 1 mL solution of isolated crosslinked tGPMVs. tGPMV was incubated for an hour at room temperature and imaged.

Image deconvolution was accomplished by the integrated deconvolution plugin (Huygens) in the Leica LAS X software. Automatic deconvolution settings were applied to slightly oversampled confocal images obtained using a 63×, NA 1.2 water immersion lens. STED microscopy was performed on an Abberior Instruments microscope with dye excitation at 640 nm and STED depletion at 775 nm using a pulsed laser source. STED alignment was accomplished using immobilized gold beads (Abberior), by adjusting the focus of the excitation beam into the center of the donut-shaped depletion laser. Corrections for mismatches between the scattering mode and the fluorescence mode were achieved using TetraSpeck (ThermoFisher) beads of four colors. Crimson beads of 28 nm diameter were used to measure the resolution of STED, which was found to be about 35 nm.[44]

FLIM Experiments: FLIM experiments were conducted on an Abberior Instruments microscope with pulsed 561 excitation. Fluorescent lifetime traces were analyzed using Becker & Hickl SPCM. The data were deconvoluted using the instrument response function (obtained by measurements of DASPI dye emission in methanol). Double-exponential fits were performed on binned data within a membrane segment as indicated by the white rectangle in Figure 3 and Figure S2 in the

**ADVANCED
SCIENCE NEWS**

www.advancedsciencenews.com

**ADVANCED
SCIENCE**
Open Access

www.advancedscience.com

Supporting Information, and the weighted average lifetime was reported. Fit was performed on the free parameters of amplitudes, lifetimes, and parameters "shift" and "scatter" using the SPCImage software. For the color-coded image in Figure 2b, each pixel was fitted to a corresponding lifetime and the lifetime histogram competed over the whole image. The histogram was then smoothed with a window size of 50 ps.

Image Quantification: Quantification of confocal images was performed using Fiji/ImageJ v. 2.0. For Figure 2e, the fluorescent signal in a circular section inside the tGPMV (radius 1 µm) and at the membrane (radius 0.1 µm) was averaged and the ratio was reported. For Figure 3b, confocal images were obtained on tubulated GUVs and a line profile was drawn across the liquid disordered outer membrane segment and a nanotube in proximity to the outer membrane segment. The confocal scanning direction was chosen to minimize polarization artifacts and only nanotubes roughly parallel to the outer membrane were considered. For each membrane segment, the peak intensity of the green and red fluorescent channels (Top flour-Chol and DiIC:18) I^{nt}_{chol}, I^{om}_{chol}, I^{nt}_{DiI}, I^{om}_{DiI} were measured. The ratio between the green/red signals in the outer membrane and nanotube were then calculated as $\frac{I^{nt}_{chol}/I^{om}_{chol}}{I^{nt}_{DiI}/I^{om}_{DiI}}$. Values close to one indicate no sorting, and values below one indicate enrichment of the DiIC:18 dye relative to TopFluor-Chol in the nanotubes. In cases where the membrane contour was poorly identified from the fluorescent images, the location of the outer membrane segment was estimated from phase contrast images.

GUV Formation: GUVs were formed by electroformation from dried lipid stacks deposited on indium tin oxide (ITO)-coated glasses as electrodes. As indicated, 8:2 DOPG:cholesterol or 3:5:2 DOPG:SM:cholesterol was deposited as a thin film (4 µL of 4×10^{-3} M lipid solution in chloroform spread on an area of about 1.5×3 cm^2, 2 h drying at vacuum) on ITO glasses. ITO glasses were then assembled with a Teflon spacer to form a chamber of 2 mL volume that was filled with a buffered sucrose solution (17 mg mL^{-1} sucrose, 2×10^{-3} M HEPES pH 7.4, containing 1×10^{-3} M EDTA). Lipids were obtained from Avanti Polar Lipids and other chemicals were obtained from Sigma. In a protocol established before, by application of a low AC-voltage during formation (640 mV$_{rms}$, 10 Hz, 2 h, 60 °C), DOPG was distributed asymmetrically in between the leaflets.[37] The lipid stocks for GUVs were doped with 0.1 mol% DiIC:18 (1,1′-dioctadecyl-3,3,3′,3′-tetramethylindodicarbocyanine-5,5′-disulfonic acid, Thermofisher) and 0.5 mol% TopFluor-Cholesterol (23-(dipyrrometheneboron difluoride)-24-norcholesterol, Avanti Polar Lipids). DOPG asymmetry decayed over time: nanotubes mostly disappeared or widened to optically resolvable diameters during storage at room temperature overnight because of passive lipid flip-flops equilibrating the membrane asymmetry. This population was then used in the "stiff elastic" experiments in Figure 3c. Before micropipette experiments, GUVs were diluted 1:10 in glucose solution (11 mg mL^{-1}).

Micropipette Experiments: Micropipettes were prepared from glass capillaries (World Precision Instruments Inc.) that were pulled using a pipette puller (Sutter Instruments, Novato, CA). Pipette tips were cut using a microforge (Narishige, Tokyo, Japan) to obtain smooth tips with inner diameter between 3 and 10 µm. Adhesion of the membrane to the pipette was prevented by incubation of the pipette tips in 1 mg mL^{-1} solution of casein or BSA (Sigma). A new pipette was used for the aspiration of each GUV. After the pipette was inserted into the observation chamber, the zero pressure across the pipette tip was attained and calibrated by watching the flow of small particles within the tip. The aspiration pressure was controlled through adjustments in the height of a connected reservoir mounted on a linear translational stage (M-531.PD; Physik Instrumente, Germany). This setup[17] allowed the pressure to increase up to 2 kPa with a resolution of 1 mPa. The pressure was changed by displacing the water reservoir at a speed of 0.01 mm s^{-1}. At every step, the system was left to equilibrate for 2–3 min before any data were recorded. Images were analyzed using the ImageJ software. The area of the membrane forming a tongue in the pipette and large spherical segment ("outer membrane") was directly measured from the membrane contour. The relative area change was calculated as $\frac{A-A_0}{A_0}$, where A is the measured vesicle area and A_0 is the spherical outer membrane segmented before aspiration.

Supporting Information

Supporting Information is available from the Wiley Online Library or from the author.

Acknowledgements

Conflict of Interest

The authors declare no conflict of interest.

Author contributions

J.S. and R.D. designed the project. T.B. performed micropipette aspiration experiments. F.S.C.L. performed dye quenching experiments. Z.Z. helped with STED experiments. J.S. performed all other experiments and initial model building. P.F. and R.L. developed the full theory. J.S., R.D. and P.F. wrote the manuscript. All authors discussed the results and commented on the manuscript.

Data Availability Statement

The data that support the findings of this study are available from the corresponding author upon reasonable request.

Keywords

[1] E. A. Evans, R. Waugh, L. Melnik, *Biophys. J.* **1976**, *16*, 585.

[2] A. Pietuch, B. R. Brückner, A. Janshoff, *Biochim. Biophys. Acta, Mol. Cell Res.* **2013**, *1833*, 712.

[3] S. Sen, S. Subramanian, D. E. Discher, *Biophys. J.* **2005**, *89*, 3203.

[4] M. P. Sheetz, *Nat. Rev. Mol. Cell Biol.* **2001**, *2*, 392.

[5] T. Baumgart, A. T. Hammond, P. Sengupta, S. T. Hess, D. A. Holowka, B. A. Baird, W. W. Webb, *Proc. Natl. Acad. Sci. USA* **2007**, *104*, 3165.

[6] J. Steinkühler, E. Sezgin, I. Urbančič, C. Eggeling, R. Dimova, *Commun. Biol.* **2019**, *2*, 337.

[7] J. Steinkühler, B. Różycki, C. Alvey, R. Lipowsky, T. R. Weikl, R. Dimova, D. E. Discher, *J. Cell Sci.* **2019**, *132*, jcs216770.

[8] R. Scott, *Science* **1976**, *194*, 743, .

[9] B. Bauer, M. Davidson, O. Orwar, *Angew. Chem., Int. Ed.* **2009**, *48*, 1656.

[10] R. Lundmark, G. J. Doherty, M. T. Howes, K. Cortese, Y. Vallis, R. G. Parton, H. T. Mcmahon, *Curr. Biol.* **2008**, *18*, 1802.

[11] W. Römer, L. Berland, V. Chambon, K. Gaus, B. Windschiegl, D. Tenza, M. R. E. Aly, V. Fraisier, J.-C. Florent, D. Perrais, C. Lamaze, G. Raposo, C. Steinem, P. Sens, P. Bassereau, L. Johannes, *Nature* **2007**, *450*, 670.

**ADVANCED
SCIENCE NEWS**

www.advancedsciencenews.com

**ADVANCED
SCIENCE**
Open Access

www.advancedscience.com

[12] Y. Li, R. Lipowsky, R. Dimova, *Proc. Natl. Acad. Sci. USA* **2011**, *108*, 4731.

[13] B. Sorre, A. Callan-Jones, J. Manzi, B. Goud, J. Prost, P. Bassereau, A. Roux, *Proc. Natl. Acad. Sci. USA* **2012**, *109*, 173.

[14] M. Simunovic, G. A. Voth, A. Callan-Jones, P. Bassereau, *Trends Cell Biol.* **2015**, *25*, 780.

[15] A. D. Skinkle, K. R. Levental, I. Levental, *Biophys. J.* **2020**, *118*, 1292.

[16] E. Sezgin, H. -. J. Kaiser, T. Baumgart, P. Schwille, K. Simons, I. Levental, *Nat. Protoc.* **2012**, *7*, 1042.

[17] T. Bhatia, J. Agudo-Canalejo, R. Dimova, R. Lipowsky, *ACS Nano* **2018**, *12*, 4478.

[18] M. Herant, V. Heinrich, M. Dembo, *J. Cell Sci.* **2006**, *119*, 1903.

[19] E. Evans, W. Rawicz, B. A. Smith, *Faraday Discuss.* **2012**, *161*, 591.

[20] M. Herant, V. Heinrich, M. Dembo, *J. Cell Sci.* **2005**, *118*, 1789.

[21] B. S. Packard, D. E. Wolf, *Biochemistry* **1985**, *24*, 5176.

[22] S. Mukherjee, T. T. Soe, F. R. Maxfield, *J. Cell Biol.* **1999**, *144*, 1271.

[23] A. Tian, T. Baumgart, *Biophys. J.* **2009**, *96*, 2676.

[24] J. B. Larsen, K. R. Rosholm, C. Kennard, S. L. Pedersen, H. K. Munch, V. Tkach, J. J. Sakon, T. Bjørnholm, K. R. Weninger, P. M. Bendix, K. J. Jensen, N. S. Hatzakis, M. J. Uline, D. Stamou, *ACS Cent. Sci.* **2020**, *6*, 1159.

[25] M. L. Torgersen, G. Skretting, B. van Deurs, K. Sandvig, *J. Cell Sci.* **2001**, *114*, 3737.

[26] M. Heinrich, A. Tian, C. Esposito, T. Baumgart, *Proc. Natl. Acad. Sci. USA* **2010**, *107*, 7208.

[27] M. Rinaldin, P. Fonda, L. Giomi, D. J. Kraft, *Nat. Commun.* **2020**, *11*, 4314.

[28] P. Fonda, M. Rinaldin, D. J. Kraft, L. Giomi, *Phys. Rev. E* **2019**, *100*, 032604.

[29] S. Baoukina, H. I. Ingólfsson, S. J. Marrink, D. P. Tieleman, *Adv. Theory Simul.* **2018**, *1*, 1800034.

[30] R. Lipowsky, *Faraday Discuss.* **2012**, *161*, 305.

[31] S. L. Veatch, P. Cicuta, P. Sengupta, A. Honerkamp-Smith, D. Holowka, B. Baird, *ACS Chem. Biol.* **2008**, *3*, 287.

[32] P. F. Almeida, *Langmuir* **2019**, *35*, 21.

[33] M. Simunovic, E. Evergren, I. Golushko, C. Prévost, H.-F. Renard, L. Johannes, H. T. Mcmahon, V. Lorman, G. A. Voth, P. Bassereau, *Proc. Natl. Acad. Sci. USA* **2016**, *113*, 11226.

[34] A. Tian, B. R. Capraro, C. Esposito, T. Baumgart, *Biophys. J.* **2009**, *97*, 1636.

[35] J. Steinkühler, R. L. Knorr, Z. Zhao, T. Bhatia, S. M. Bartelt, S. Wegner, R. Dimova, R. Lipowsky, *Nat. Commun.* **2020**, *11*, 905.

[36] R. Dasgupta, M. S. Miettinen, N. Fricke, R. Lipowsky, R. Dimova, *Proc. Natl. Acad. Sci. USA* **2018**, *115*, 5756.

[37] J. Steinkühler, P. De Tillieux, R. L. Knorr, R. Lipowsky, R. Dimova, *Sci. Rep.* **2018**, *8*, 11838.

[38] C. C. Vequi-Suplicy, K. A. Riske, R. L. Knorr, R. Dimova, *Biochim. Biophys. Acta, Biomembr.* **2010**, *1798*, 1338.

[39] B. Sorre, A. Callan-Jones, J.-B. Manneville, P. Nassoy, J.-F. Joanny, J. Prost, B. Goud, P. Bassereau, *Proc. Natl. Acad. Sci. USA* **2009**, *106*, 5622.

[40] J. J. Thottacherry, A. J. Kosmalska, A. Kumar, A. S. Vishen, A. Elosegui-Artola, S. Pradhan, S. Sharma, P. P. Singh, M. C. Guadamillas, N. Chaudhary, R. Vishwakarma, X. Trepat, M. A. Del Pozo, R. G. Parton, M. Rao, P. Pullarkat, P. Roca-Cusachs, S. Mayor, *Nat. Commun.* **2018**, *9*, 4217.

[41] T. Portet, S. E. Gordon, S. L. Keller, *Biophys. J.* **2012**, *103*, L35.

[42] W. Rawicz, K. C. Olbrich, T. Mcintosh, D. Needham, E. Evans, *Biophys. J.* **2000**, *79*, 328.

[43] K. Otsuka, C. M. Wayman, *Shape Memory Materials*, Cambridge University Press, Cambridge **1999**.

[44] D. Roy, J. Steinkühler, Z. Zhao, R. Lipowsky, R. Dimova, *Nano Lett.* **2020**, *20*, 3185.

ADVANCED SCIENCE
Open Access

Supporting Information

Superelasticity of Plasma- and Synthetic Membranes Resulting from Coupling of Membrane Asymmetry, Curvature, and Lipid Sorting

Jan Steinkühler,* Piermarco Fonda, Tripta Bhatia, Ziliang Zhao, Fernanda S. C. Leomil, Reinhard Lipowsky, and Rumiana Dimova*

Supplemental Information

Super-elasticity of plasma- and synthetic membranes resulting from coupling of
membrane asymmetry, curvature and lipid sorting

Jan Steinkühler[1,2*], Piermarco Fonda[1], Tripta Bhatia[1,3], Ziliang Zhao[1], Fernanda S. C. Leomil[1,4],
Reinhard Lipowsky[1], Rumiana Dimova[1*]

[1] Theory and Bio-Systems, Max Planck Institute of Colloids and Interfaces, Science Park Golm,
14424 Potsdam, Germany
[2] Current address: Department of Biomedical Engineering, Northwestern University, Evanston,
IL 60657, USA
[3] Department of Physical Sciences, Indian Institute of Science Education and Research Mohali,
Sector 81, Knowledge City, S. A. S. Nagar, Manauli 140306, India
[4] Departamento de Biofísica, Universidade Federal de São Paulo, 043039-032, Brazil

Supplemental Figures
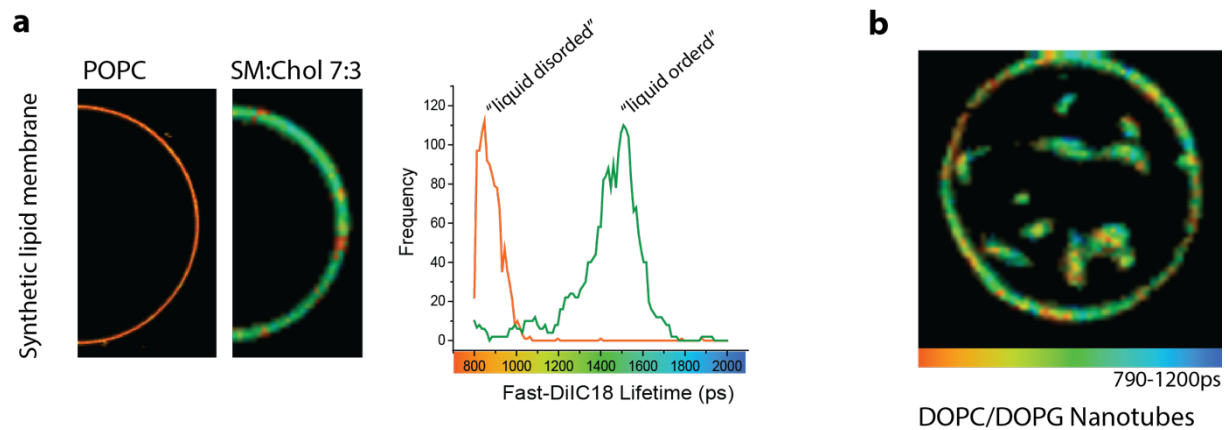
Fig. S1 – Control FLIM measurements. a) Fast-DiI fluorescent lifetime is sensitive to
membrane order in synthetic POPC "liquid-discorded" (left) and liquid-ordered egg
sphingomyelin:cholestetrol (right) 7:3 membranes. GUVs were prepared at the indicated
lipid concentrations as described in the main text with 0.1 mol% Fast-DiI dye. Both signals
show representative GUVs from separate experiments of each composition. Color code
shows FLIM lifetime. b) In homogenous DOPC:DOPG GUVs (see main text method) which
exhibit nanotubes of the same composition as the outer membrane segment, Fast-DiI does
not have a significant shift in fluorescent lifetime, indicating that Fast-DiI is not sensitive to
membrane curvature alone.
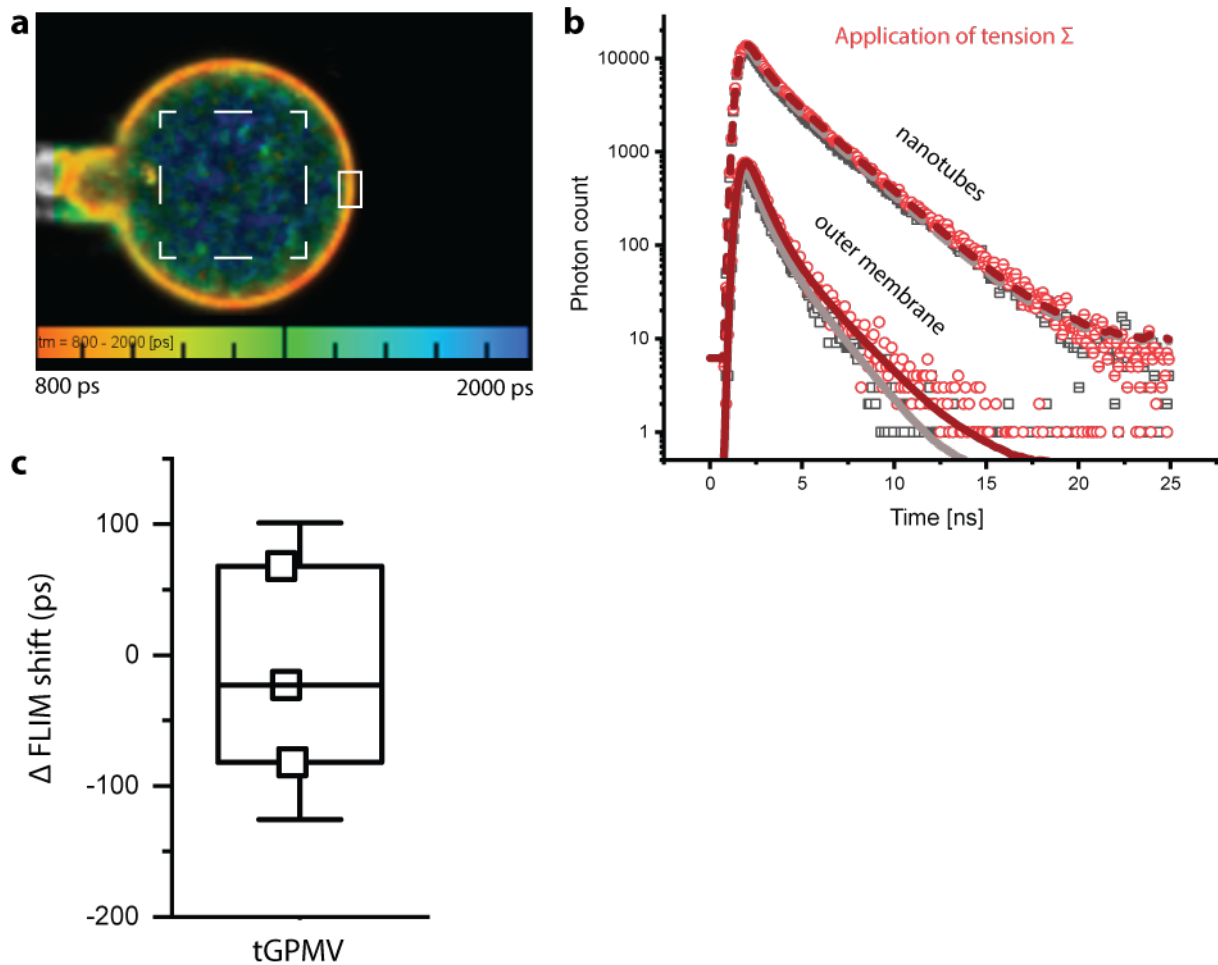
Fig S2 – Quantification of the negligible tension-induced shift of the average fluorescence lifetime of the nanotube network in tGPMVs. a) White square and rectangle indicate segments used for binning of nanotube lifetime data and subsequent fitting. Color code shows fluorescence lifetime and demonstrates the large variability measured in the nanotube network. b) Example traces obtained from binned signal (square/rectangle in panel a). Solid curves (data for outer membrane) and dashed curves (nanotubes) are 2-component exponential decay fits. Traces in red/dark red correspond to signal from the same segment after aspiration with a small tension Σ. In this example, the tension-induced shift in outer membrane fluorescence lifetime corresponds to about Δ ≈ 93 ps, while it was not resolvable for the nanotubes. c) Analysis of the shift in the average nanotube lifetime after application of a small tension difference 0.7 ± 0.3 mN/m for n=3 repeats.

Fig S3 – Results of quenching 3/5/2 DOPG/eggSM/chol GUVs doped with tail-labeled NBD-PG. The reference signal of unquenched vesicles was normalized to 100 intensities units. Addition of a membrane impermeable NBD quenching agent to the GUV external solution shifted the fluorescent intensities to a mean of 38 intensity units (see SI Methods for details). These results indicate accumulation of DOPG in the outer bilayer leaflet during the GUV formation procedure and establishes the 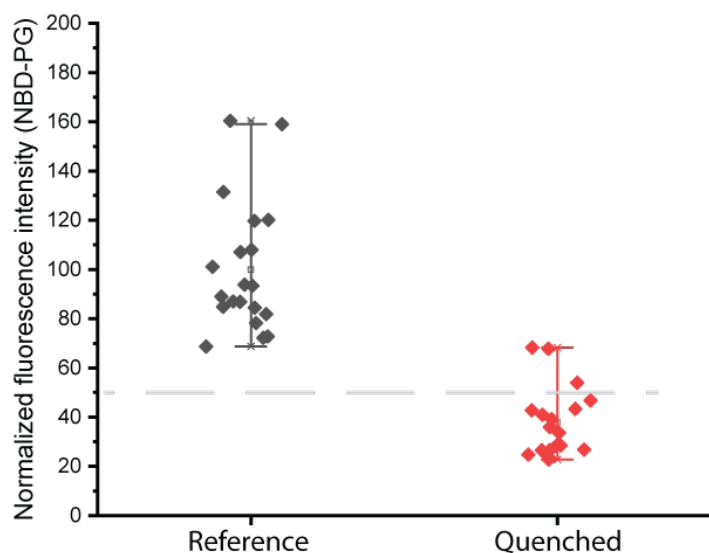molecular basis for the spontaneous curvature of tGUVs. Gray dashed line indicates 50 intensity units. For details of the assay and sorting of DOPG see (Steinkühler et al., 2018).

Supplemental Methods

Quenching Experiments

For each experiment, we first prepared a fresh 100 mM stock solution of sodium dithionite (Sigma) in 1M Tris-HCl buffer. 3/5/2 DOPG/eggSM/chol GUV with 1 mol% NBD-PG (1-oleoyl-2-[12-[(7-nitro-2-1,3-benzoxadiazol-4-yl)amino]dodecanoyl]-sn-glycero-3-[phospho-rac-(1-glycerol)] (ammonium salt) (Avanti Polar Lipids)) (for other details see main text methods) were grown using electro-formation in 200 mM sucrose HEPES pH 7.4 + 0.1 mM EDTA buffer, similar to the protocol in Ref. (Steinkühler et al., 2018). Then, 1.5 µL of this quenching buffer was pipetted into 58.5 µL of vesicle suspension in 200 mM glucose buffer (40 µL of glucose + 18.5 µL of GUV). The solution was gently stirred to ensure homogenous distribution of the quenching agent. The vesicles were then incubated for 5 minutes and consecutively diluted in 200 mM glucose buffer (to a final volume of 300 µL). From this final mixture, 60 µL was used for observation. For each population (non-quenched and quenched), at least 18 GUVs were imaged at the equatorial plane. The membrane intensity was assessed from the average of 4 peak maxima from the line profiles, drawn in the 4 brightest regions of the membrane.

Steinkühler, J., De Tillieux, P., Knorr, R. L., Lipowsky, R., & Dimova, R. (2018). Charged giant unilamellar vesicles prepared by electroformation exhibit nanotubes and transbilayer lipid asymmetry. *Scientific Reports*. https://doi.org/10.1038/s41598-018-30286-z

Estimation of the chemically-induced super-elastic coefficient

Even though GPMV membranes are complex mixtures of several components, the essential mechanism through which the aspiration-induced mixing of differently curved domains generates the super-elastic response can be captured by a simple binary model. Therefore, for simplicity, we treat the tGPMV membrane as a two-component fluid consisting of two generic lipids species A and B.

The membrane is stable and there is no significant lipid exchange with the solvent, so both individual lipid numbers N^A and N^B are conserved quantities. We define the global membrane composition as

$$\Phi = \frac{N^A}{N^A + N^B} \,, \tag{S1}$$

which quantifies the relative number of A lipids in the membrane. The relative number of B lipids is given by $1 - \Phi$.

After tubulation, the tGPMV is at equilibrium with its surroundings and comprises primarily two environments: the nanotubes and the outer membrane domains. We label quantities relative to each of these domains respectively with nt and om. The two domains have different sizes, which we quantify via their areas $\mathcal{A}_{\mathrm{nt}}$ and $\mathcal{A}_{\mathrm{om}}$ and enclosed volumes V_{nt} and V_{om}. We assume that both the total area $\mathcal{A}_{\mathrm{tot}}$ and the total volume V_{tot} of the tGPMV are fixed quantities at equilibrium. Therefore, the relationships

$$\mathcal{A}_{\mathrm{tot}} = \mathcal{A}_{\mathrm{nt}} + \mathcal{A}_{\mathrm{om}} \,, \qquad V_{\mathrm{tot}} = V_{\mathrm{om}} - V_{\mathrm{nt}} \,, \tag{S2}$$

must hold. Note that because the nanotubes are inside the tGPMV, the volume V_{nt} must be *subtracted* from the outer segment one, so that $V_{\mathrm{tot}} < V_{\mathrm{om}}$. We also assume, for simplicity, that the average area per lipid, a, is the same for both species and is not changed significantly during aspiration. Similarly to Eq. (S1) we define the relative area fraction occupied by the outer membrane domain

$$y = \frac{\mathcal{A}_{\mathrm{om}}}{\mathcal{A}_{\mathrm{nt}} + \mathcal{A}_{\mathrm{om}}} \,, \tag{S3}$$

so that the nanotubes occupy an area $(1 - y)\mathcal{A}_{\mathrm{nt}}$.

We also need to introduce the local composition variables

$$\Phi_{\mathrm{nt}} = \frac{N_{\mathrm{nt}}^A}{N_{\mathrm{nt}}^A + N_{\mathrm{nt}}^B} \,, \qquad \Phi_{\mathrm{om}} = \frac{N_{\mathrm{om}}^A}{N_{\mathrm{om}}^A + N_{\mathrm{om}}^B} \,, \tag{S4}$$

which give the relative amount of A lipids in the nanotubes and the outer membrane. These compositions must match the global lipid fraction Eq. (S1) when weighted with the respective membrane area. By combining Eq. (S3) and Eq. (S4) together with $N^A = N_{\mathrm{nt}}^A + N_{\mathrm{om}}^A$ and $N^B = N_{\mathrm{nt}}^B + N_{\mathrm{om}}^B$ we obtain the further constraint

$$\mathcal{A}_{\mathrm{nt}}\Phi_{\mathrm{nt}} + \mathcal{A}_{\mathrm{om}}\Phi_{\mathrm{om}} = \mathcal{A}_{\mathrm{tot}}\Phi \,. \tag{S5}$$

Note that this expression entangles Φ_{om}, Φ_{nt} and the domain areas: a generic shape change of a domain affects its chemical nature.

The general form of the free energy

The free energy of the system is an extensive quantity, so we can decompose it as

$$F = F_{\mathrm{nt}} + F_{\mathrm{om}} \,, \tag{S6}$$

where $F_{\mathrm{nt,om}}$ are the local free energies of the respective domains. In principle, we should also include a line term quantifying the energy of the domain boundaries where the composition smoothly interpolates between Φ_{om} and Φ_{nt}. Since the length of this interface-like portion is expected to be small and not to change significantly during aspiration, we will ignore such a contribution in the following.

In general, both terms in Eq. (S6) can be written as surface integrals of local densities, which must depend on local intensive variables:

$$F_{\mathrm{nt}} = \int_{\mathcal{A}_{\mathrm{nt}}} \mathrm{d}A f(\Phi_{\mathrm{nt}}, M_{\mathrm{nt}}) \,, \qquad F_{\mathrm{om}} = \int_{\mathcal{A}_{\mathrm{om}}} \mathrm{d}A f(\Phi_{\mathrm{om}}, M_{\mathrm{om}}) \,, \tag{S7}$$

where M_{nt} and M_{om} are the local mean curvatures of the membrane[1]. For the explicit dependence of f on the geometry, we choose a generalised Canham-Helfrich density

$$f(\Phi, M) = e(\Phi) + 2\kappa(\Phi)\left(M - m(\Phi)\right)^2 , \tag{S8}$$

where $e(\Phi)$ is the chemical free energy density per unit area, which, in general, will contain both internal and entropic (i.e. temperature dependent) contributions, while $\kappa(\Phi)$ and $m(\Phi)$ are respectively the composition-dependent bending modulus and spontaneous curvature.

It is precisely the coupling terms in Eq. (S8) between Φ and M that allow, at equilibrium, the two membrane domains to sustain different compositions, i.e. to have $\Phi_{\mathrm{om}} \neq \Phi_{\mathrm{nt}}$. Conversely, for homogeneous vesicles where $\Phi_{\mathrm{om}} = \Phi_{\mathrm{nt}} = \Phi$ (see Eq. (S5)), the free energy Eq. (S6) would reduce to the usual spontaneous curvature model of lipid membranes.

The equilibrium conditions for the tGPMV can be obtained by minimizing Eq. (S7) with respect to compositions and geometric variables. However, note that the variables entering Eq. (S6) are not all independent from each other: the global membrane composition, the total area and the total volume are all fixed quantities (see Eq. (S2) and Eq. (S5)). Finding minima of Eq. (S6) is thus a constrained minimisation problem which can be solved with the aid of Lagrange multipliers. We thus must consider the generalised free energy

$$G = G_{\mathrm{nt}} + G_{\mathrm{om}} , \tag{S9}$$

with

$$G_{\mathrm{nt}} = F_{\mathrm{nt}} + (\Sigma - \lambda\Phi_{\mathrm{nt}})\,\mathcal{A}_{\mathrm{nt}} + \Delta P V_{\mathrm{nt}} , \tag{S10a}$$

$$G_{\mathrm{om}} = F_{\mathrm{om}} + (\Sigma - \lambda\Phi_{\mathrm{om}})\,\mathcal{A}_{\mathrm{om}} - \Delta P V_{\mathrm{om}} , \tag{S10b}$$

where λ is the Lagrange multiplier enforcing Eq. (S5), Σ is the Lagrange multiplier enforcing the total area to be $\mathcal{A}_{\mathrm{tot}}$ and $\Delta P = P_{\mathrm{in}} - P_2$ is the pressure differential between the inside and the outside of the tGPMV.

Equilibrium configurations are those that satisfy $\delta G = 0$, where variations can be carried out independently for variables relative to each domain. These derivatives can be of two kinds: with respect to the chemical compositions or with respect to membrane shape, and will produce two sets of equations, to which we refer respectively as "chemical" and "mechanical" equilibrium conditions.

Before aspiration, the solution of these equations determines the equilibrium values Φ_{nt} and Φ_{om}. Because of the composition-curvature couplings in Eq. (S8), we expect these to be different from each other. It is then useful to introduce the composition difference

$$\Delta\Phi = \Phi_{\mathrm{nt}} - \Phi_{\mathrm{om}} , \tag{S11}$$

which vanishes only for homogeneous vesicles.

Lipid and area recruitment upon aspiration

We model the tGPMV aspiration process as shown in Fig. S4. As the outer membrane is exposed to two different external pressures (denoted P_1 and P_2), its shape deviates significantly from a sphere. We capture the essential features of the tGPMV geometry as shown in Fig. S4b: the outer membrane segment consists of the union a spherical outer segment of radius R_{v} with a cylindrical portion inside the pipette of radius R_{p} and length L_{p} ending on a tongue-like spherical cap[2] of radius R_{t}. At the initial aspiration stage there is no cylindrical segment (i.e. $L_{\mathrm{p}} = 0$) and the tongue radius decreases from $R_{\mathrm{t}} = R_{\mathrm{om}}$ (the original outer sphere radius) towards its minimum value $R_{\mathrm{t}} = R_{\mathrm{p}}$. In homogeneous tubulated vesicles it is precisely at this point that the droplet-like instability develops, as the suction pressure crosses a critical threshold and the whole vesicle suddenly flows inside the pipette [2]. In the present case, however, such instability is absent and the vesicle can sustain larger pressures so to have $L_{\mathrm{p}} > 0$ while maintaining $R_{\mathrm{t}} = R_{\mathrm{p}}$.

To avoid confusion with quantities referring to the non-aspirated tGPMV we will denote any variable relative to the aspirated vesicle with a prime $'$, so that e.g. $\mathcal{A}'_{\mathrm{om}}$ refers to the area of the aspirated vesicle.

Since $\mathcal{A}'_{\mathrm{om}} > \mathcal{A}_{\mathrm{om}}$, we define the area difference $\Delta\mathcal{A} = \mathcal{A}'_{\mathrm{om}} - \mathcal{A}_{\mathrm{om}} > 0$. From Fig. 2a we see that the super-elastic response happens for relative area changes, $\Delta\mathcal{A}/\mathcal{A}_{\mathrm{om}}$, in the range of $5 - 25\%$. Using the surface parametrization sketched in Fig. S4b, we can calculate exactly every geometrical aspects of the aspiration process, including $\Delta\mathcal{A}$. At the initial stage of the aspiration we have $L_{\mathrm{p}} = 0$ and the area increase is due only to the decrease of the tongue radius towards R_{p}. Fig. S4c

---

[1]A completely general energy density would also depend on the local Gaussian curvature K. However, for simplicity and since linear terms in K are topological, we neglect such contributions here.

[2]The shape of the tongue cannot be exactly spherical [1], although this would lead to only minor corrections to Eq. (S23).
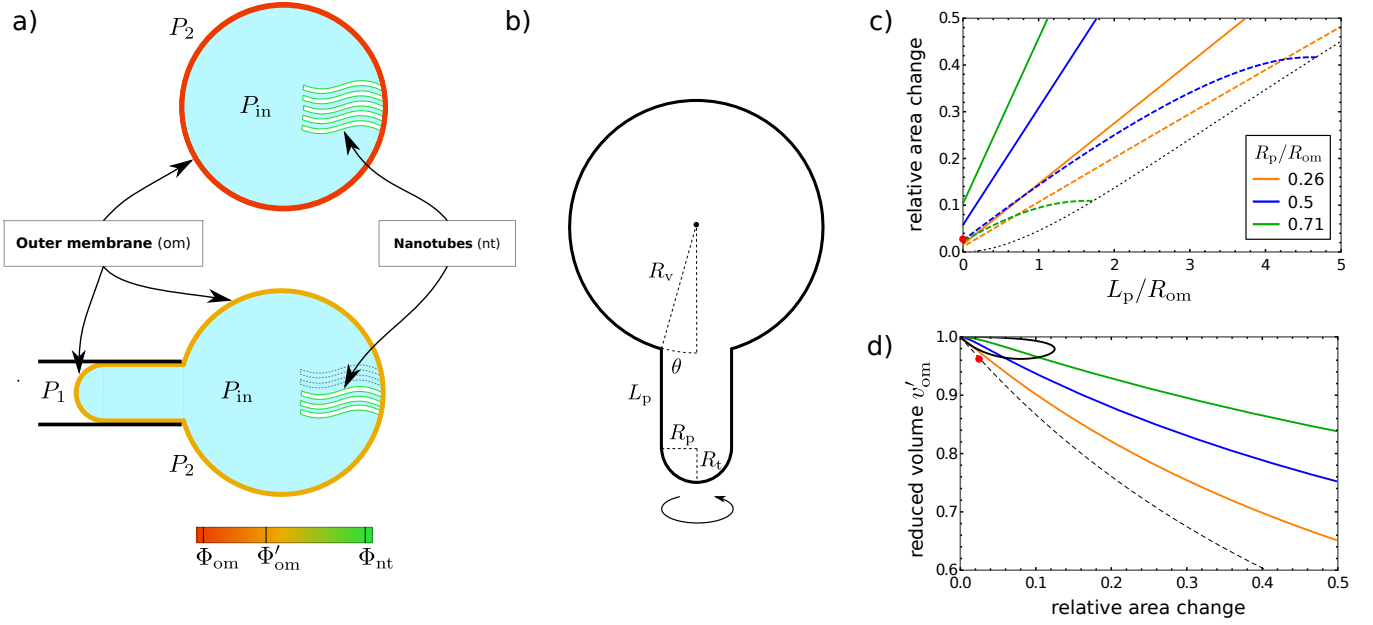
Figure S4: **a)** Cartoon showing the effect of aspiration on tGPMV shape and composition. *Top:* before aspiration, the tGPMV comprises two domains: an outer sphere of radius R_{om} and composition Φ_{om} (red), and the nanotubes of cross-sectional radius R_{nt} and composition Φ_{nt} (green). The tubes are inward pointing, so $V_{tot} < V_{om}$. *Bottom:* during aspiration new lipids are recruited from nanotubes (dashed outline) so that the outer segment changes shape but also composition, shifting to a value Φ'_{om} (orange), closer to Φ_{nt}. **b)** The geometry of the outer segment during aspiration is well approximated by the union of two spherical caps and a cylindrical segment. The angle θ subtends a cone such that $R_p = \sin\theta R_v$. Initial aspiration has $L_p = 0$ and $R_t > R_p$, until when $R_t = R_p$ and L_p starts increasing. **c)** Relative area increase $\Delta\mathcal{A}/\mathcal{A}_{om}$ for the shape shown in **b** as a function of the aspirated length, from Eq. (S17). We model this aspiration either at constant volume (dashed lines) or at constant outer sphere radius $R_v = R_{om}$ (solid lines). The colours refer to different relative pipette sizes as shown in the legend. The dotted line is the maximal L_p for constant volume aspiration, beyond which the tGPMV is entirely suctioned. **d)** Reduced volume $v'_{om} = 6\sqrt{\pi}V'_{om}(\mathcal{A}'_{om})^{-3/2}$ as a function of area increase, with the same colour coding as in **c**: constant $R_v = R_{om}$ aspirations (solid lines) discriminate between different R_p, while constant volume aspirations collapse on the single dashed curve $(\Delta\mathcal{A}/\mathcal{A}_{om})^{-3/2}$. The solid black line shows the boundary between the initial aspiration regime with $R_t > R_p$ and the suction with $L_p \neq 0$. The red dot shows the maximum achievable $\Delta\mathcal{A}/\mathcal{A}_{om}$ with $L_p = 0$ for constant volume aspirations.

and Fig. S4d show how this initial phase is not relevant for the experimentally measured area changes, as for a wide range of relative pipette sizes $R_\mathrm{p}/R_\mathrm{om}$ the maximal increases at this stage are always below $\sim 5\%$. Dashed and continuous lines in these plots refer to two different assumptions on the outer membrane volume V'_om during aspiration: the former refer to constant outer radius deformations, i.e. $R_\mathrm{v} = R_\mathrm{om}$ is kept constant while V'_om increases; the latter refers to constant volume aspirations where $V'_\mathrm{om} = V_\mathrm{om}$ is kept constant and the outer sphere radius decreases, $R_\mathrm{v} < R_\mathrm{om}$. Experimentally it is hard to distinguish between these two limiting cases: on the one hand, the outer membrane segment radius seems to be constant within optical resolution, while on the other one would expect no significant volume change due to smallness of $V_\mathrm{nt} \propto R_\mathrm{nt}^2$. Likely, the experimental setup lies somewhere in between these two limits. Regardless, Fig. S4c and Fig. S4d clearly show that we can ignore the initial stage of aspiration and focus on the later stage with $L_\mathrm{p} > 0$ and $R_\mathrm{t} = R_\mathrm{p}$, as we shall do in the following.

Given the measured low value of the elastic modulus, we can safely assume that the average area per lipid a is also constant, which otherwise would lead to a significantly stiffer elastic response, as is the case for non-tubulated vesicles (see Figs. 2b and 3c). This means that the observed $\Delta\mathcal{A}$ is entirely due to lipid recruitment from the nanotubes, and thus represents an *area transfer* between domains. From this, it follows that the the total tGPMV area is constant during aspiration, and to every area increase of the om domain there must be a corresponding area decrease of the nt domain, namely

$$\mathcal{A}_\mathrm{nt} \quad \to \quad \mathcal{A}'_\mathrm{nt} = \mathcal{A}_\mathrm{nt} - \Delta\mathcal{A}\,, \tag{S12a}$$

$$\mathcal{A}_\mathrm{om} \quad \to \quad \mathcal{A}'_\mathrm{om} = \mathcal{A}_\mathrm{om} + \Delta\mathcal{A}\,, \tag{S12b}$$

so that $\mathcal{A}_\mathrm{tot}$ remains unchanged. Due to the multi-component nature of the membrane, this area transfer implies that the composition of outer membrane can change during aspiration, as shown in Fig. 2c. If lipid recruitment from the nanotubes proceeds uniformly, i.e. the amount of A and B lipids transferred from the nanotubes to the outer membrane is uniquely determined by Φ_nt, the recruited area will contain $2\Delta\mathcal{A}\Phi_\mathrm{nt}/a$ type A lipids and $2\Delta\mathcal{A}(1 - \Phi_\mathrm{nt})/a$ type B lipids. We can drop this assumption at the expense of introducing a further variable quantifying the relative mole fraction $\Phi_{\Delta\mathcal{A}}$ in the transferred area $\Delta\mathcal{A}$. This could explain the shift in tubes composition observed during aspiration (see the shift of the FAST-DiI fluorescence lifetime distribution in Fig. 2c of the main text), but it is not necessary for the sake of the argument presented here. For the time being, we thus take $\Phi_{\Delta\mathcal{A}} = \Phi_\mathrm{nt}$ as a simplifying assumption.

It then follows that compositions change as

$$\Phi_\mathrm{nt} \quad \to \quad {\Phi_\mathrm{nt}}' = \Phi_\mathrm{nt}\,, \tag{S13a}$$

$$\Phi_\mathrm{om} \quad \to \quad {\Phi_\mathrm{om}}' = \Phi_\mathrm{om} + \Delta\Phi\frac{\Delta\mathcal{A}}{\mathcal{A}'_\mathrm{om}}\,, \tag{S13b}$$

where $\Delta\Phi = \Phi_\mathrm{nt} - \Phi_\mathrm{om}$ is the pre-aspiration equilibrium difference defined in Eq. (S11). the value of Φ_om is pushed towards Φ_nt (see Fig. S4a), and Eq. (S13b) clearly shows how the aspiration process entangles a *geometric* variation to a change in the *chemical composition* of the membrane. The outer membrane local curvature M'_om of the aspirated tGPMV is no longer constant, but rather a piece-wise constant function. Because of the curvature-composition couplings one would expect also Φ'_om to be a piece-wise constant function over the three portions of the aspirated tGPMV membrane as well, so that Eq. (S13b) would quantify only an average compositional shift. In the experiments, however, no significant inhomogeneity in the outer segment has been observed. We can explain this by noting that the nanotubes typical curvature $M_\mathrm{nt} = 1/2R_\mathrm{nt}$ is at least two orders of magnitude larger than any characteristic curvature of the outer membrane (either $1/R_\mathrm{om}$, $1/R_\mathrm{v}$ or $1/R_\mathrm{p}$). We infer that the coupling mechanism inducing $\Delta\Phi \neq 0$ is too weak to generate a measurable inhomogeneity in the different portions of the outer membrane. We thus consider both the tongue and the external spherical cap being formed by a uniform membrane of compositions Φ'_om.

In order to link the applied pressure to geometric and compositional changes, we must minimise the free energy. Note that now, because we are considering Φ_nt a fixed quantity, we must rewrite the constraint Eq. (S5) accordingly. Using Eq. (S13) and Eq. (S12) we have

$$\mathcal{A}_\mathrm{tot}\Phi = \mathcal{A}'_\mathrm{nt}\Phi'_\mathrm{nt} + \mathcal{A}'_\mathrm{om}\Phi'_\mathrm{om} = \mathcal{A}'_\mathrm{om}(\Phi'_\mathrm{om} - \Phi_\mathrm{nt}) + \mathcal{A}_\mathrm{tot}\Phi_\mathrm{nt}\,, \tag{S14}$$

where the last term in the right-hand side is a constant. At this point, we can ignore the nanotube domain and focus on the outer membrane segment. We thus consider only the second term in Eq. (S9):

$$G_\mathrm{om} = F_\mathrm{om} + (\Sigma - \lambda(\Phi'_\mathrm{om} - \Phi_\mathrm{nt}))\,\mathcal{A}'_\mathrm{om} - \sum_i (P_\mathrm{in} - P_i)V'_{\mathrm{om},i}\,, \tag{S15}$$

where

$$F_\mathrm{om} = \sum_i \mathcal{A}'_{\mathrm{om},i}\,f(\Phi'_\mathrm{om}, M'_{\mathrm{om},i})\,, \tag{S16}$$

7

and the sums span over the three constant curvature portions of the outer membrane domain, with $\mathcal{A}'_{\text{om},i}$ and $V'_{\text{om},i}$ being their respective areas and volumes such that $\sum_i \mathcal{A}'_{\text{om},i} = \mathcal{A}'_{\text{om}}$ and $\sum_i V'_{\text{om},i} = V'_{\text{om}}$. P_i are the external pressures to which each portion is subject to, while there is a single composition Φ'_{om} over the whole domain. In Eq. (S15), the Lagrange multiplier Σ enforces constraint Eq. (S12b) while λ enforces Eq. (S14).

Specifically, the areas and curvatures of these portions are, past the initial aspiration stage, respectively $1/R_{\text{v}}$ and $2\pi R_{\text{v}}(1 + \cos\theta)$ on the outer spherical segment, $1/2R_{\text{p}}$ and $2\pi L_{\text{p}} R_{\text{p}}$ on the cylinder and $1/R_{\text{p}}$ and $2\pi R_{\text{p}}$ on the tongue ($\theta = \arcsin R_{\text{p}}/R_{\text{v}}$ is the subtended angle of the pipette on the outer spherical segment). Using the surface parametrization of the aspirated outer membrane shown in Fig. S4b, the expression for the whole outer membrane domain area is

$$\mathcal{A}'_{\text{om}} = 2\pi R_{\text{v}}^2 \left(1 + \cos\theta + \sin^2\theta + \frac{L_{\text{p}}}{R_{\text{v}}} \sin\theta \right) , \tag{S17}$$

so that the relative area increase is

$$\frac{\Delta\mathcal{A}}{\mathcal{A}_{\text{om}}} = \frac{R_{\text{v}}^2}{2R_{\text{om}}^2} \left(1 + \cos\theta + \sin^2\theta + \frac{L_{\text{p}}}{R_{\text{v}}} \sin\theta - 2\frac{R_{\text{om}}^2}{R_{\text{v}}^2} \right) . \tag{S18}$$

While this expression formally depends on two geometric ratios, $R_{\text{om}}/R_{\text{v}}$ and $L_{\text{p}}/R_{\text{v}}$, $\Delta\mathcal{A}$ truly depends on a single degree of freedom (e.g. the length L_{p}), since we still need to fix whether V_{om} or R_{om} is kept constant during aspiration. These different choices lead to two distinct expressions for $\Delta\mathcal{A}$ as a function of L_{p}, as shown respectively by the dashed and solid lines in Fig. S4c.

With the explicit form Eq. (S15) we can now carry out variations with respect to composition and shape on each portions of the outer membrane domain.

Chemical equilibrium   Taking a derivative with respect to Φ'_{om} of G_{om} in Eq. (S15) leads to

$$\frac{1}{\mathcal{A}'_{\text{om}}} \sum_i \mathcal{A}'_{\text{om},i} \left. \frac{\partial f}{\partial \Phi} \right|_{\Phi = \Phi'_{\text{om}}, M = M'_{\text{om},i}} = \lambda , \tag{S19}$$

which for the Canham-Helfrich density Eq. (S8) becomes

$$\partial_\Phi \left(e(\Phi'_{\text{om}}) + 2\kappa(\Phi'_{\text{nt}}) m(\Phi'_{\text{nt}})^2 \right) + \frac{h_\kappa}{\mathcal{A}'_{\text{om}}} \partial_\Phi \kappa(\Phi'_{\text{om}}) - \frac{R_{\text{v}} h_m}{\mathcal{A}'_{\text{om}}} \partial_\Phi (\kappa(\Phi'_{\text{om}}) m(\Phi'_{\text{om}})) = \lambda , \tag{S20}$$

where $\mathcal{A}'_{\text{om}}$ is given by Eq. (S17) and we defined the two dimensionless auxiliary functions

$$h_\kappa(\theta, L_{\text{p}}/R_{\text{v}}) = 4\pi \left(2 + \cos\theta + \frac{L_{\text{p}}}{4 R_{\text{v}} \sin\theta} \right) , \tag{S21a}$$

$$h_m(\theta, L_{\text{p}}/R_{\text{v}}) = 8\pi \left(1 + \cos\theta + \sin\theta + \frac{L_{\text{p}}}{2 R_{\text{v}}} \right) . \tag{S21b}$$

Mechanical equilibrium   The cylindrical part of the outer membrane is in direct contact with the pipette wall which, being a solid, can exert an arbitrary reaction pressure P_{wall} on the membrane, counterbalancing any mechanical force. Therefore this portion will not provide any physically relevant information about the the suction process and we can focus on the two other parts of the domain: the outer segment and the tongue. Since both are spherical caps, their shape equations are

$$P_{\text{in}} - P_2 = 2\frac{\Sigma + e(\Phi'_{\text{om}}) - \lambda(\Phi'_{\text{om}} - \Phi_{\text{nt}}) + 2\kappa(\Phi'_{\text{om}}) m(\Phi'_{\text{om}})^2}{R_{\text{v}}} - 4\frac{\kappa(\Phi'_{\text{om}}) m(\Phi'_{\text{om}})}{R_{\text{v}}^2} , \tag{S22a}$$

$$P_{\text{in}} - P_1 = 2\frac{\Sigma + e(\Phi'_{\text{om}}) - \lambda(\Phi'_{\text{om}} - \Phi_{\text{nt}}) + 2\kappa(\Phi'_{\text{om}}) m(\Phi'_{\text{om}})^2}{R_{\text{p}}} - 4\frac{\kappa(\Phi'_{\text{om}}) m(\Phi'_{\text{om}})}{R_{\text{p}}^2} , \tag{S22b}$$

which can be combined into a single equation

$$\frac{\Delta P}{2\left(\frac{1}{R_{\text{p}}} - \frac{1}{R_{\text{v}}} \right)} = \Sigma + e(\Phi'_{\text{om}}) - \lambda(\Phi'_{\text{om}} - \Phi_{\text{nt}}) + 2\kappa(\Phi'_{\text{om}}) m(\Phi'_{\text{om}})^2 - 2\kappa(\Phi'_{\text{om}}) m(\Phi'_{\text{om}}) \left(\frac{1}{R_{\text{p}}} + \frac{1}{R_{\text{v}}} \right) , \tag{S23}$$

where $\Delta P = P_2 - P_1$ is the difference between the pressure inside the pipette and the external environment. This equation generalises the well-known Laplace relation for homogeneous vesicles [3], as the Lagrange multiplier λ depends non-trivially on the geometric degrees of freedom of the vesicle via Eq. (S20). One recovers the standard result by setting $\lambda = 0$ and removing any Φ'_{om} dependence.

Solving for λ in Eq. (S20) and substituting back into Eq. (S23) leads to

$$\frac{\Delta P}{2\left(\frac{1}{R_{\mathrm{p}}} - \frac{1}{R_{\mathrm{v}}}\right)} = \hat{\Sigma}'_{\mathrm{om}} - 2\kappa(\Phi'_{\mathrm{om}})m(\Phi'_{\mathrm{om}})\left(\frac{1}{R_{\mathrm{p}}} + \frac{1}{R_{\mathrm{v}}}\right) -$$
$$(\Phi'_{\mathrm{om}} - \Phi_{\mathrm{nt}})\left[\frac{h_\kappa}{\mathcal{A}'_{\mathrm{om}}}\partial_\Phi\kappa(\Phi'_{\mathrm{om}}) - \frac{R_{\mathrm{v}}h_m}{\mathcal{A}'_{\mathrm{om}}}\partial_\Phi(\kappa(\Phi'_{\mathrm{om}})m(\Phi'_{\mathrm{om}}))\right], \quad \text{(S24)}$$

where the auxiliary functions h_κ and h_m are defined in Eq. (S21) and we defined

$$\hat{\Sigma}'_{\mathrm{om}} = \Sigma + e(\Phi'_{\mathrm{om}}) + 2\kappa(\Phi'_{\mathrm{om}})m(\Phi'_{\mathrm{om}})^2 - (\Phi'_{\mathrm{om}} - \Phi_{\mathrm{nt}})\partial_\Phi\left(e(\Phi'_{\mathrm{om}}) + 2\kappa(\Phi'_{\mathrm{om}})m(\Phi'_{\mathrm{om}})^2\right). \quad \text{(S25)}$$

Chemically-generated elastic modulus   Within the assumptions of our model, Eq. (S24) is an exact relation that links the pressure difference ΔP to the measured area increase $\Delta\mathcal{A}$. Note that the dependence on $\Delta\mathcal{A}$ enters this expression both through Φ'_{om} (via Eq. (S13b)) and through the geometric variables L_{p} and $\mathcal{A}'_{\mathrm{om}}$ (respectively via Eq. (S18) and via Eq. (S17))[3].

From Fig. 2a it is clear that the aspiration tension depends, in first approximation, linearly on $\Delta\mathcal{A}/\mathcal{A}_{\mathrm{om}}$. Given that the measured values of $\Delta\mathcal{A}$ are always below $\sim 25\%$, we can expand Eq. (S24) for small area increases, so to collect information on the coefficient of this linear dependence. For simplicity, we focus now on aspirations that keep the outer membrane segment radius constant, i.e. $R_{\mathrm{v}} = R_{\mathrm{om}}$. Then, L_{p} is related to $\Delta\mathcal{A}$ via Eq. (S18) as

$$L_{\mathrm{p}} = R_{\mathrm{v}}\left(\frac{2}{\sin\theta}\frac{\Delta\mathcal{A}}{\mathcal{A}_{\mathrm{om}}} - \cos\theta\tan\theta/2\right). \quad \text{(S26)}$$

By plugging this expression and Eq. (S13b) back into Eq. (S24) and expanding to first order in the area increase, we obtain

$$\frac{\Delta P}{2\left(\frac{1}{R_{\mathrm{p}}} - \frac{1}{R_{\mathrm{v}}}\right)} \simeq \Sigma_{\mathrm{app}} + K_{\mathrm{app}}\frac{\Delta\mathcal{A}}{\mathcal{A}_{\mathrm{om}}} + O(\Delta\mathcal{A}^2), \quad \text{(S27)}$$

where Σ_{app} is a tension-like term that collects all $\Delta\mathcal{A}$-independent quantities, while K_{app} is the *chemically-generated elastic modulus*, with general structure

$$K_{\mathrm{app}} = \Delta\Phi\left(\frac{j_m^{(1)}}{R_{\mathrm{v}}}\partial_\Phi(\kappa(\Phi_{\mathrm{om}})m(\Phi_{\mathrm{om}})) + \frac{j_\kappa^{(1)}}{R_{\mathrm{v}}^2}\partial_\Phi\kappa(\Phi_{\mathrm{om}})\right) +$$
$$\Delta\Phi^2\left(\partial_\Phi^2(e(\Phi_{\mathrm{om}}) + 2\kappa(\Phi_{\mathrm{om}})m(\Phi_{\mathrm{om}})^2) + \frac{j_m^{(1)}}{R_{\mathrm{v}}}\partial_\Phi^2(\kappa(\Phi_{\mathrm{om}})m(\Phi_{\mathrm{om}})) + \frac{j_\kappa^{(1)}}{R_{\mathrm{v}}^2}\partial_\Phi^2\kappa(\Phi_{\mathrm{om}})\right), \quad \text{(S28)}$$

where we defined the four auxiliary functions

$$j_m^{(1)}(\theta) = 2\left(1 + 2\cos\theta + \sin\theta - 2\cot\theta/2\right), \quad \text{(S29a)}$$
$$j_\kappa^{(1)}(\theta) = \frac{1}{4\sin\theta}\left(-7 + 7\cos 2\theta + 2\cos 3\theta - 2\cot\theta/2\right), \quad \text{(S29b)}$$
$$j_m^{(2)}(\theta) = -\left(2 + 2\cos\theta + \sin\theta + \tan\theta/2\right), \quad \text{(S29c)}$$
$$j_\kappa^{(2)}(\theta) = \frac{7}{4} + \cos\theta + \frac{1}{4(1 + \cos\theta)}. \quad \text{(S29d)}$$

which depend only on θ and are displayed in Fig. S5.

As reported in the main text, the measured value for K_{app} from tGPMV aspiration is $3.1 \pm 0.2\mathrm{mN/m}$. Typical parameter values are $m \sim 1/(100\mathrm{nm})$ for the spontaneous curvature, $\kappa \sim 10^{-19}J$ for the bending rigidity. The typical size of a tGPMV

---

[3] Note that for constant volume aspirations, where $V'_{\mathrm{om}} = V_{\mathrm{om}}$ is maintained throughout suction, also R_{v} depends on $\Delta\mathcal{A}$, although this dependence cannot explain the relatively large area increase shown in Fig. 2a, nor the magnitude of K_{app}.
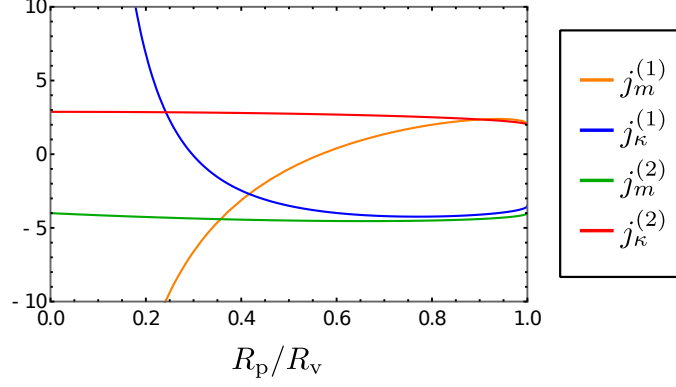
Figure S5: The auxiliary functions $j_\beta^{(\alpha)}$ appearing in Eq. (S28), quantifying the geometric contributions to the chemically-generated elastic modulus K_{app}, as a function of $\sin\theta = R_{\mathrm{p}}/R_{\mathrm{v}}$ for aspirations at constant $R_{\mathrm{v}} = R_{\mathrm{om}}$.

is $R_{\mathrm{om}} \sim 10\mu$m. Roughly, the derivatives of $\kappa(\Phi_{\mathrm{om}})$ or $m(\Phi_{\mathrm{om}})$ with respect to concentrations quantify *differences* of these material parameters between membrane consisting of pure phases (i.e. bilayers made entirely of either A or B lipids). Hence, it is tempting to estimate their values to be at most of the same order of magnitude as the values for pure membranes. Furthermore, from Fig. S5 we see that the magnitude of the functions appearing in Eq. (S29) is, in modulus, consistently below 10 for $R_{\mathrm{p}} \gtrsim R_{\mathrm{v}}/5$. Since $|\Delta\Phi| < 1$, we infer that all terms appearing in Eq. (S28) besides the one depending on $e(\Phi_{\mathrm{om}})$ will contribute to K_{app} with magnitudes of the order at most of $\sim 10\mu$N/m, i.e. about two orders of magnitude less than the measured value. We therefore conclude that the main contribution to the chemically-generated elastic modulus must come from the internal energy, i.e.:

$$K_{\mathrm{app}} \simeq \Delta\Phi^2 \frac{\partial^2 e(\Phi_{\mathrm{om}})}{\partial\Phi^2}\,. \tag{S30}$$

It is not possible to find a more precise estimate for K_{app} without choosing an explicit form for the free energy density Eq. (S8), in particular of the exact dependence on Φ of the curvature coupling functions $\kappa(\Phi_{\mathrm{om}})$ and $m(\Phi_{\mathrm{om}})$.

An explicit model

In our derivation we did not have to provide any detail about the explicit *composition* dependence of the free energy density $f(\Phi, M)$ appearing in Eq. (S8). In fact, this was not necessary in order to prove that, when the tGPMV is aspirated into the pipette, the relative area increase induces a shift in the outer segment composition $\Phi_{\mathrm{om}} \to \Phi_{\mathrm{om}}{}'$ (see Eq. (S13b)). In turn, this compositional shift generates an elastic term which opposes any further area increase. Such term, quantified in first approximation by the "apparent" elastic modulus K_{app} appearing in Eq. (S28), is the only one that sources a linear response (i.e. a term proportional to $\Delta\mathcal{A}/\mathcal{A}_{\mathrm{om}}$) to the applied pressure differential $\Delta P = P_2 - P_1$. We can argue that it is precisely this term that avoids the "droplet-like" instability observed in homogeneous vesicles [2], since now the elastic term can counterbalance arbitrarily high ΔP values, trying to push the outer tGPMV back into its spherical configuration prior to aspiration.

What we cannot do without an explicit expression for $f(\Phi, M)$, however, is to provide an exact quantitative estimate for K_{app} in terms of the membrane material parameters. It is thus instructive to choose a specific form for the free energy density - and specifically for the three functions $e(\Phi)$, $m(\Phi)$ and $\kappa(\Phi)$ -, and show how all the physically relevant quantities, namely the equilibrium composition difference $\Delta\Phi$, the total tension $\hat{\Sigma}_{\mathrm{om}}$ and the elastic modulus K_{app} can be computed explicitly.

We need first to fix an explicit form of the curvature-independent free energy density per unit area $e(\Phi)$: a typical choice for qualitative descriptions of binary mixtures is the mean-field theory of two-dimensional lattice gas theory. Then, following e.g. [4], we set

$$e(\Phi) = u(\Phi) - k_B T s(\Phi)\,, \tag{S31}$$

with the internal energy density $u(\Phi)$ and entropy density $s(\Phi)$

$$u(\Phi) = \frac{\omega}{a}\Phi(1-\Phi)\,, \tag{S32a}$$

$$s(\Phi) = -\frac{1}{a}\left(\Phi\ln\Phi + (1-\Phi)\ln(1-\Phi)\right)\,, \tag{S32b}$$

where $\omega > 0$ is the net $A - B$ lipid interaction strength, which promotes demixing, and T is the vesicle temperature. A thermodynamic system described by Eq. (S32) can undergo phase separation for subcritical temperatures $T < T_c = \frac{w}{2k_B}$ and composition values within the binodal interval.

Furthermore, we choose to model the curvature-composition interaction by allowing the spontaneous curvature to be a linear function

$$m(\Phi) = m_B + \Delta m \ \Phi \,, \tag{S33}$$

where $\Delta m = m_A - m_B$, with m_A (m_B) the spontaneous curvature of a membrane consisting purely of A (B) lipids. Conversely, we take for simplicity the bending modulus to be the same for both species, i.e. we set $\kappa(\Phi) = \kappa$. For a general discussion on possible alternatives to Eq. (S33) see [4].

From Eq. (S32) and Eq. (S33) we get the explicit form of the free energy density Eq. (S8):

$$f(\Phi, M) = \frac{\omega}{a}\Phi(1 - \Phi) + \frac{k_B T}{a}\left(\Phi \ln \Phi + (1 - \Phi)\ln(1 - \Phi)\right) + 2\kappa\left(M - m_B - \Delta m \ \Phi\right)^2 \,. \tag{S34}$$

The first derivative of $f(\Phi, M)$ with respect to composition is then

$$\frac{\partial f}{\partial \Phi} = \frac{\omega}{a}(1 - 2\Phi) - \frac{2k_B T}{a}\tanh^{-1}(1 - 2\Phi) - 4\kappa\Delta m\left(M - m_B - \Delta m \ \Phi\right) \,. \tag{S35}$$

A curvature coupling of the form Eq. (S33) produces a non-homogeneous vesicle *prior to aspiration*. To see this, we take the derivative with respect to Φ_{om} and Φ_{nt} of Eq. (S9), which leads to the chemical equilibrium condition

$$\frac{\omega}{a}(1 - 2\Phi_{\mathrm{om}}) - \frac{2k_B T}{a}\tanh^{-1}(1 - 2\Phi_{\mathrm{om}}) - 4\kappa\Delta m\left(M_{\mathrm{om}} - m_B - \Delta m \ \Phi_{\mathrm{om}}\right)$$

$$= \frac{\omega}{a}(1 - 2\Phi_{\mathrm{nt}}) - \frac{2k_B T}{a}\tanh^{-1}(1 - 2\Phi_{\mathrm{nt}}) - 4\kappa\Delta m\left(M_{\mathrm{nt}} - m_B - \Delta m \ \Phi_{\mathrm{nt}}\right) \,, \tag{S36}$$

where $M_{\mathrm{om}} = 1/R_{\mathrm{om}}$ and $M_{\mathrm{nt}} = -1/(2R_{\mathrm{nt}})$ are respectively the curvatures of the spherical outer membrane and the cylindrical nanotubes. We can cast this equation in a simpler form by using Eq. (S5), which implies

$$\Phi_{\mathrm{om}} = \Phi - (1 - y)\Delta\Phi \,, \tag{S37a}$$

$$\Phi_{\mathrm{nt}} = \Phi + y\Delta\Phi \,, \tag{S37b}$$

where Φ is the global mole fraction defined in Eq. (S1) and $y = \mathcal{A}_{\mathrm{om}}/\mathcal{A}_{\mathrm{tot}}$ is the outer segment area fraction. Plugging Eq. (S37) back into Eq. (S36) we get

$$\frac{w}{a}\Delta\Phi + \frac{k_B T}{2a}\ln\left(\frac{\Phi - (1 - y)\Delta\Phi}{\Phi + y\Delta\Phi}\frac{1 - \Phi - y\Delta\Phi}{1 - \Phi + (1 - y)\Delta\Phi}\right) = 2\kappa\Delta m\left(\Delta m\Delta\Phi - M_{\mathrm{nt}} + M_{\mathrm{om}}\right) \,. \tag{S38}$$

Although it is not possible to find an analytic solution to this equation, we can find an approximate value for weak curvature-composition couplings. In this case we can expanding Eq. (S38) for small Δm and get

$$\Delta\Phi \simeq \kappa\Delta m(M_{\mathrm{nt}} - M_{\mathrm{om}})\frac{a}{k_B T}\left(\frac{1}{4(1 - \Phi)\Phi} - \frac{T_c}{T}\right)^{-1} + O(\Delta m^2) \,, \tag{S39}$$

where M_{nt} and M_{om} are the local mean curvatures of the two domains. As expected, $\Delta\Phi$ vanishes for $\Delta m = 0$. It also vanishes when the geometry of the vesicle is homogeneous ($M_{\mathrm{om}} = M_{\mathrm{nt}}$) or when the mole fraction is saturated to extremal values ($\Phi = 0, 1$), so that the membrane consists of a single component. In general, Eq. (S39) shows how a curvature-dependent free energy necessarily enforces a difference of equilibrium compositions between different membrane domains - without the need to invoke thermodynamic phase-separation even at subcritical temperatures $T < T_c$ [4].

We can now compute the chemically-generated modulus K_{app} for this specific model. First, note that since $m(\Phi_{\mathrm{om}})$ is a linear function and κ is a constant, the general expression Eq. (S28) simplifies considerably:

$$K_{\mathrm{app}} = \Delta\Phi\frac{\kappa\Delta m}{R_{\mathrm{v}}}j_m^{(1)} + \Delta\Phi^2\left[\frac{k_B T}{a}\left(\frac{1}{\Phi - (1 - y)\Delta\Phi} + \frac{1}{1 - \Phi + (1 - y)\Delta\Phi}\right) - 4\left(\frac{k_B T_c}{a} - \kappa\Delta m^2\right)\right] \,. \tag{S40}$$

Now, as shown in Fig. S5, $|j_m^{(1)}(\theta)| < 10$ for $R_{\mathrm{p}} \gtrsim R_{\mathrm{v}}/5$. If we use the approximate values $|\Delta m| \simeq 1/(100\mathrm{nm})$, $\kappa \simeq 10^{-19}J$ and $R_{\mathrm{v}} \simeq 10\mu\mathrm{m}$, we get $|\frac{\kappa\Delta m}{R_{\mathrm{v}}}j_m^{(1)}| \simeq 1\mu\mathrm{N/m}$. Similarly, the $\kappa\Delta m^2$ term will have a magnitude of at most $\simeq 10\mu\mathrm{N/m}$.

We thus see that both these terms cannot produce significant contributions to K_{app}, whose measured value is much larger, of the order of a few mN/m.

What is left to consider in Eq. (S40) is the contribution originating from the thermodynamic free energy $e(\Phi_{\mathrm{om}})$. For small $\Delta\Phi$ this can be approximated as

$$K_{\mathrm{app}} \simeq \Delta\Phi^2 \frac{k_B T}{a} \left(\frac{1}{\Phi(1-\Phi)} - 4\frac{T_c}{T} \right) + O(\Delta m^3) \,, \tag{S41}$$

which, at leading order, depends on Δm only through $\Delta\Phi$ (see Eq. (S39)). We can take some putative values for the domain compositions in order to obtain an estimate for K_{app}: consider a situation where the nanotubes are almost purely made by A molecules, i.e. $\Phi_{\mathrm{nt}} \simeq 1$. From the sorting diagram in Fig. 3b, we can postulate that the outer segment composition is about $\Phi_{\mathrm{om}} \simeq 0.65$, so that $\Delta\Phi \simeq 0.35$. Assuming both environments have roughly the same relative area, we can estimate the total mole fraction to lie somewhere in between, say at $\Phi \simeq 0.85$. We then have that Eq. (S41) becomes

$$K_{\mathrm{app}} \simeq \left(6.5 - 3.4\frac{T_c}{T} \right) \mathrm{mN/m} \,. \tag{S42}$$

which would require $\omega \simeq 2.1 k_B T$ (or equivalently $T \sim 0.96 T_c$) in order for this expression to reproduce the measured value $K_{\mathrm{app}} \simeq 3.1 \mathrm{mN/m}$, with a lipid cross sectional area of $a \simeq 0.6 \mathrm{nm}^2$.

References

[1] J.-B. Fournier and P. Galatola. Corrections to the Laplace law for vesicle aspiration in micropipettes and other confined geometries. *Soft Matter*, 4(12):2463, 2008.

[2] Tripta Bhatia, Jaime Agudo-Canalejo, Rumiana Dimova, and Reinhard Lipowsky. Membrane Nanotubes Increase the Robustness of Giant Vesicles. *ACS Nano*, 12(5):4478–4485, may 2018.

[3] Reinhard Lipowsky. Understanding Membranes and Vesicles: A Personal Recollection of the Last Two Decades. In *Physics of Biological Membranes*, pages 3–44. Springer International Publishing, Cham, 2018.

[4] Piermarco Fonda, Melissa Rinaldin, Daniela J. Kraft, and Luca Giomi. Thermodynamic equilibrium of binary mixtures on curved surfaces. *Physical Review E*, 2019.